Gondwana Research 39 (2016) 165–179

Contents lists available at ScienceDirect

Gondwana Research

journal homepage: www.elsevier.com/locate/gr

Petrogenesis and geodynamic implications of the Late Carboniferous felsic volcanics in the Bogda belt, Chinese Northern Tianshan

Wei Xie [a,b,*], Yi-Gang Xu [a], Zhen-Yu Luo [a], Hai-Quan Liu [c], Lu-Bing Hong [a], Liang Ma [a]

[a] State Key Laboratory of Isotope Geochemistry, Guangzhou Institute of Geochemistry, Chinese Academy of Sciences, Guangzhou 510640, China
[b] College of Oceanography, Hohai University, Nanjing 210098, China
[c] Key Laboratory of Marginal Sea Geology, Guangzhou Institute of Geochemistry, Chinese Academy of Sciences, Guangzhou 510640, China

ARTICLE INFO

Article history:
Received 15 November 2015
Received in revised form 11 July 2016
Accepted 11 July 2016
Available online 27 August 2016

Handling Editor: I. Safonova

Keywords:
Late Carboniferous
Partial melting
Magma mingling
Arc felsic volcanics
Chinese Northern Tianshan

ABSTRACT

An integrated study on petrology and geochemistry has been carried out on the Late Carboniferous I-type felsic volcanics of the Liushugou Formation in the Bogda belt to constrain the late Paleozoic tectonic evolution of the Bogda belt. The felsic volcanics were dated to be 315 to 319 Ma and are composed of trachy-andesite–trachyte ignimbrites and rhyolite lavas. They are in conformable contact with high-Al basalt. The eruption of the felsic volcanics and high-Al basalt is not bimodal volcanism, but is related to bimodal magma (basaltic and rhyolitic magmas). MELTS modeling and comparison with previous basaltic melting experiments indicate that the felsic volcanics are likely produced by partial melting of hydrated mafic crust rather than fractional crystallization of high-Al basalt. It is also supported by relatively large amounts of felsic volcanics to high-Al basalts and remarkably different incompatible element ratios (e.g., Th/Zr, Nb/Zr and U/Zr) of the rocks. The Bogda felsic volcanics have positive $\varepsilon_{Nd(t)}$ values (6.2–7.4), low Pb isotopes and low zircon saturation temperatures, consistent with a derivation from a juvenile crust in an arc setting. The intermediate ignimbrites display melting–mingling textures and abundant feldspar aggregates and have various δEu ratios, indicating that magma mingling and feldspar fractionation processes may have played an important role in the genesis of the ignimbrites. In contrast, the Early Permian felsic rocks in this region are of post-collisional A-type. We therefore propose that the Bogda belt was an island arc in the Late Carboniferous and then switched to a post-collisional setting in the Early Permian due to the arc–arc collision at the end of the Late Carboniferous.

1. Introduction

Arc magmatism is a principal process in continental creation at least in the Phanerozoic (Davidson and Arculus, 2006). The Bogda–(Harlik) belt in the northern margin of Chinese North Tianshan (Fig. 1) is considered to be an ancient arc system between the Juggar Basin to the north and the Tu–Ha Basin to the south (Ma et al., 1997; Xiao et al., 2004; Chen et al., 2013; Xie et al., 2016a). Thus, the magmatism in the Bogda belt may record pivotal information of Phanerozoic, especially Carboniferous–Permian, crustal growth of the Central Asian Orogenic Belt (CAOB) (Sengör et al., 1993; Jahn et al., 2000; Xiao et al., 2004; Windley et al., 2007; Safonova et al., 2011; Wilhem et al., 2012; Xiao et al., 2013). However, the tectonic evolution of this region in Carboniferous–Permian remains debated on 1) a post-collisional orogenic belt as Paleo-Tianshan Ocean closed at the end of Early Carboniferous (Han et al., 2010; Chen et al., 2011; Han et al., 2011), 2) a Carboniferous–Permian continental rift associated with a mantle plume (Gu et al., 2000, 2001; Xia et al., 2008, 2012), and 3) a Carboniferous island arc system switched to a post-collisional orogenic belt in Permian (Ma et al., 1997; Laurent-Charvet et al., 2003; Xiao et al., 2004; Yuan et al., 2010; Shu et al., 2011; Xie et al., 2016a).

Magmatism in this region may provide clues to evaluate among these competing models. Most previous studies focused on the effusive lavas or intrusions in the Bogda belt, whereas ignimbrites are less concerned. Ignimbrites actually occur worldwide in many volcanic provinces of different ages and embrace almost all magma compositions except for the most mafic end members (Walker, 1983; Branney and Kokelaar, 2002). The ignimbrite formed by pyroclastic flow is denoted as pyroclastic rock, which is mainly composed of breccia, tuff, lithic clast, fiamme (plastic fragment), fragmentized crystal and glass shard matrix whether it is welded or not (Sparks et al., 1973).

In this paper, we present petrology and geochemistry of the Late Carboniferous intermediate ignimbrites and rhyolite lavas in the Bogda belt. They have highly variable compositions from trachy-andesite to rhyolite, and likely formed by crustal melting, extensive

* Corresponding author at: State Key Laboratory of Isotope Geochemistry, Guangzhou Institute of Geochemistry, Chinese Academy of Sciences, 510640 Wushan, Guangzhou, China.
E-mail address: air_weixie@gig.ac.cn (W. Xie).

http://dx.doi.org/10.1016/j.gr.2016.07.005
1342-937X/

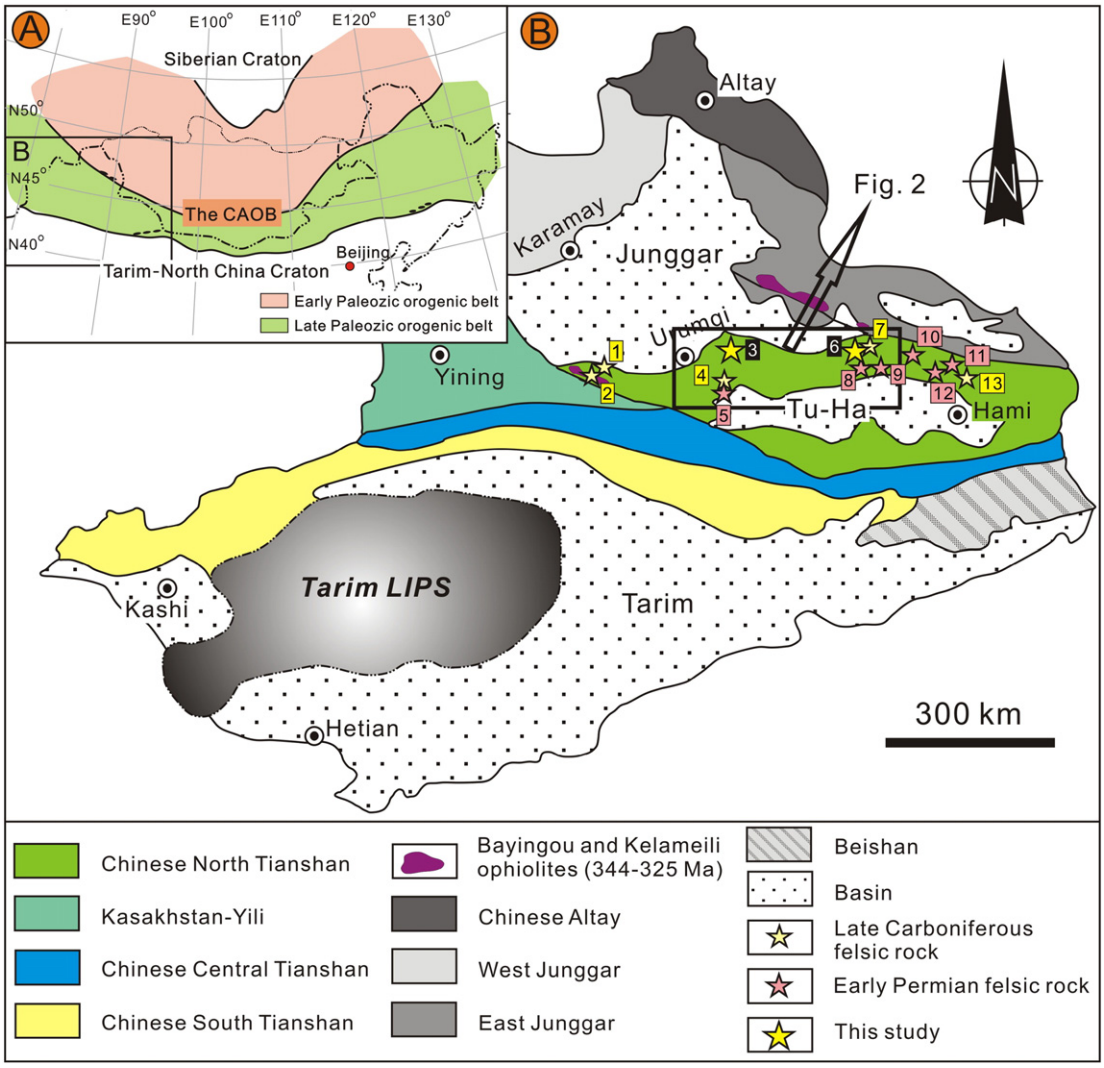

Fig. 1. (A) Schematic geologic map of the Central Asian orogenic belt (CAOB); (B) Simplified tectonic sketch map of most part of Xinjiang province, NW China modified after Pirajno et al. (2008), Wang et al. (2011) and Xiao et al. (2013). The details of the Late Carboniferous and Early Permian felsic rocks in the Bogda-Harlik belt are given in Table 1.

magma mingling and feldspar fractionation processes in an island arc setting. Integration of the Late Carboniferous and Early Permian volcanic rocks in this region indicates that the Carboniferous island arc system was followed by a post-collisional orogenic system in the Early Permian.

2. Geochronology and petrology of the felsic volcanics

Although some authors thought that the Harlik domain was not the equivalent of Bogda and North Tianshan but a unit attached to the northern block of the "Mongolian system" (Charvet et al., 2007, 2011; Chen et al., 2014), many researchers believed that the Harlik and Bogda domains were considered to be a Devonian–Carboniferous arc system (Ma et al., 1997; Xiao et al., 2004; Sun et al., 2005; Li et al., 2006; Yuan et al., 2010; Zhang et al., 2016). The oldest sedimentary strata merely occur in the Harlik Mountains (Sun et al., 2005; Yuan et al., 2010) and are composed of the Ordovician to Silurian marine clastic rock and tuff, which are interlayered with limestone and subordinate basalt in local places (Huangcaopo Group; Ma, 1999). Devonian marine–terrigenous tuffaceous sandstone and volcanic rock also mainly occur in the Harlik Mountains. The Carboniferous strata mainly exposed in the Bogda Mountains (Fig. 2A) and are in fault contact with the Devonian strata and are further divided into three formations, namely the Lower Carboniferous Qijiaojing Formation, the Upper Carboniferous Liushugou and Qijiagou formations (BGMRXUAR, 1993; Gu et al., 2001; Liang et al., 2011). The Lower and Upper Carboniferous formations are separated by regional faults. The Lower Carboniferous formation consists mainly of marine volcanic ignimbrite, tuffaceous sandstone, bimodal volcanic lava, while the Upper Carboniferous formation is dominated by marine (pillow) basaltic lava, felsic ignimbrite and lava, with minor sandstone and siltstone. The Permian strata are unconformably underlain by the Carboniferous rocks. Permian strata are mainly composed of terrestrial conglomerate, sandstone, siliceous mudstone intercalated with bimodal volcanic lava. Jurassic clastic sediment occurs in the southeast of this region and is unconformably underlain by the Permian strata (Carroll et al., 1990; BGMRXUAR, 1993).

Two stratigraphic columnar-sections, the Tianchi and Dashitou sections in the northern Bogda belt, have been investigated (Fig. 2). These two columnar-sections are ~1000 m thick and are occupied by the Upper Carboniferous Liushugou Formation (BGMRXUAR, 1993; Gu et al., 2001; Liang et al., 2011), which is mainly composed of High-Al basalt (HAB), intermediate ignimbrite, rhyolite lava and volcanic breccia. The intermediate ignimbrite is about 500 m thick and is composed of trachy-andesite and trachyte (see geochemistry section below). The ignimbrites have ~80 vol% volcanics (except for volcanic

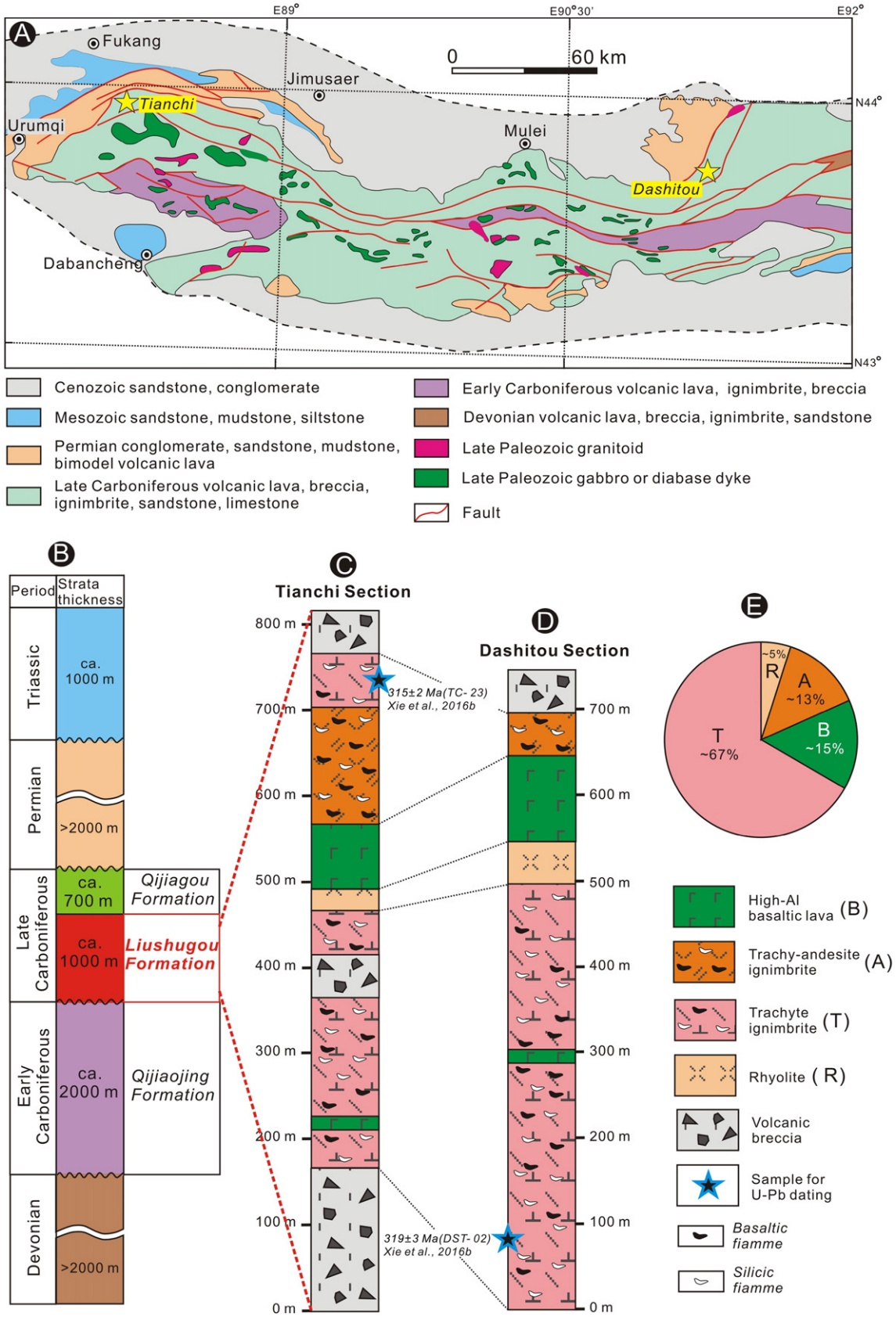

Fig. 2. (A) Geological map of the Bogda belt at the north margin of the Chinese North Tianshan, modified after Chen et al. (2011) and Zhao et al. (2014). (B) Simplified stratigraphy column from Devonian to Triassic in the Bogda area (modified after BGMRXUAR, 1993). (C, D) Two composite stratigraphy columns of the Liushugou Formation in the Bogda area, showing the relationship of the felsic volcanics and high-Al basaltic lava (HAB). (E) Pie chart of the total average volume proportions of the volcanics (except the breccias) from the Liushugou Formation.

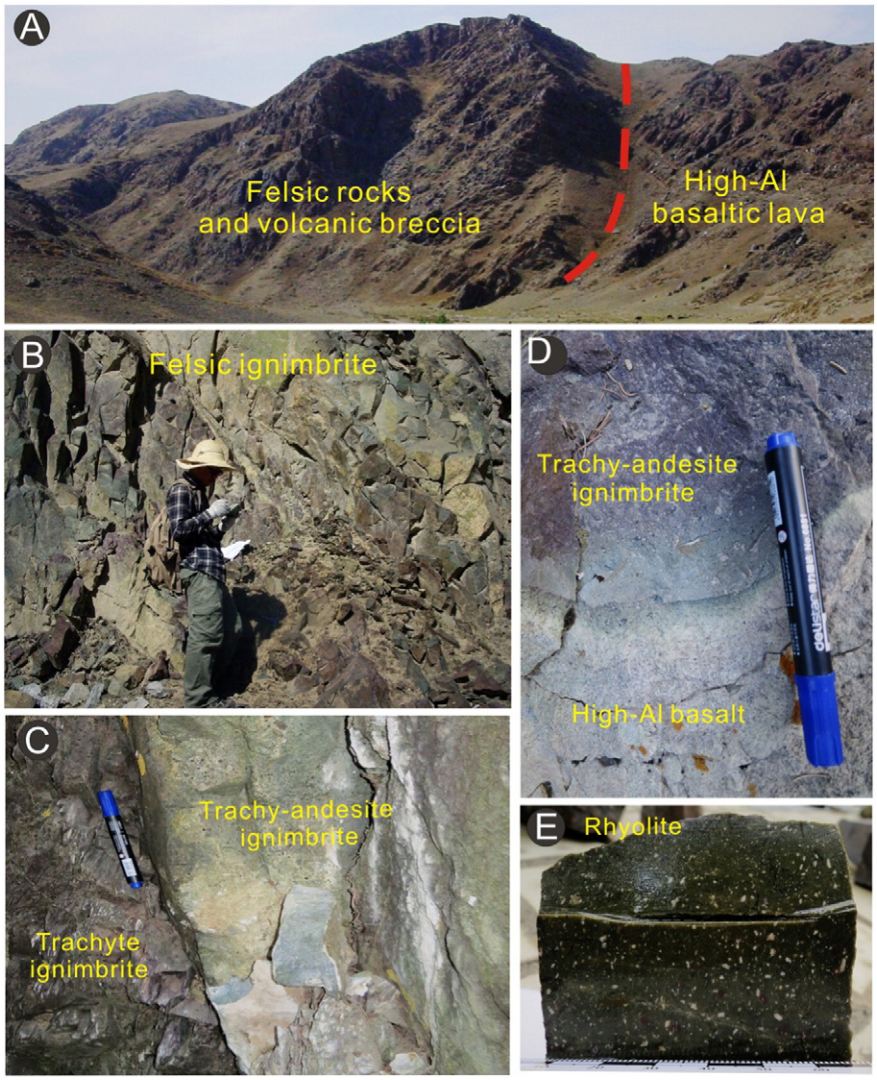

Fig. 3. (A, B) Outcrops of the Bogda Late Carboniferous volcanics from the Liushugou Formation. (C, D) Field photos showing the conformable contacts with each other. (E) Hand specimen of a rhyolite showing a typical porphyritic texture.

breccias), especially the trachyte ignimbrite (~67 vol%; Fig. 2E). They are in conformable contact with HAB and rhyolites (Fig. 3). The trachyte ignimbrites were dated to be 315 ± 2 Ma and 319 ± 3 Ma by SHRIMP technique (Xie et al., 2016b), which are interpreted as the eruption age of the volcanics of the Liushugou Formation.

Trachy-andesite ignimbrites have matrix and fiamme proportions different from trachyte ignimbrites (Fig. 4). The matrix (50–70%) is composed of feldspar microlite and black glass or tiny feldspathic minerals. The fiamme (5–15%) mainly contains basaltic and silicic fiamme. The basaltic fiammes are composed of tiny plagioclase microlite and black glass matrix, whereas silicic fiammes are composed of transparent microlite and cryptocrystals such as feldspar and quartz. Generally, trachy-andesite ignimbrite contains more basaltic fiammes and less silicic fiammes than trachyte ignimbrite. Crystal fragments or aggregates make up 20–40% of trachy-andesite and trachyte ignimbrites and have grain size ranging from 0.5 to 1 mm, and they are mainly composed of euhedral and resorbed feldspar with minor quartz, pyroxene, chlorite and Fe–Ti oxides. Thus, these ignimbrites are composed of typical magmatic materials except minor unknown lithic clasts (<1%).

The rhyolite lava is about 30 m thick and contains ~5 vol% volcanics (except for volcanic breccias), 10–20% phenocrysts (0.5–1 mm) and 80–90% matrix. Phenocrysts are mainly composed of quartz and feldspar with minor Fe–Ti oxides. The matrix is composed of cryptocrystalline feldspathic minerals. The rhyolite is directly overlain by high-Al basalts. The rhyolite and basalt are associated with intermediate ignimbrites and make up at least two volcanic cycles (Fig. 2). The suite of the Late Carboniferous volcanics of the Liushugou Formation is different from the Early Permian bimodal volcanics which lack the intermediate composition and are intercalated within sandstone and siliceous mudstone (Chen et al., 2011).

3. Analytical techniques

Nineteen fresh ignimbrite and four rhyolite samples were analyzed for major and trace element and Nd–Pb isotopic compositions. Whole-rock major oxide analyses were carried out using X-ray fluorescence spectrometry (XRF, Rigaku ZSX-100e) on fused glass beads at Guangzhou Institute of Geochemistry, Chinese Academy of Sciences (GIGCAS) and analytical uncertainties are mostly between 1 and 5%. Trace element concentrations were determined by utilization of PerkinElmer Sciex ElAN 6000 ICP-–MS. The analytical precision is better than 5% for elements >10 ppm, less than 8% for those <10 ppm, and about 10% for transition metals.

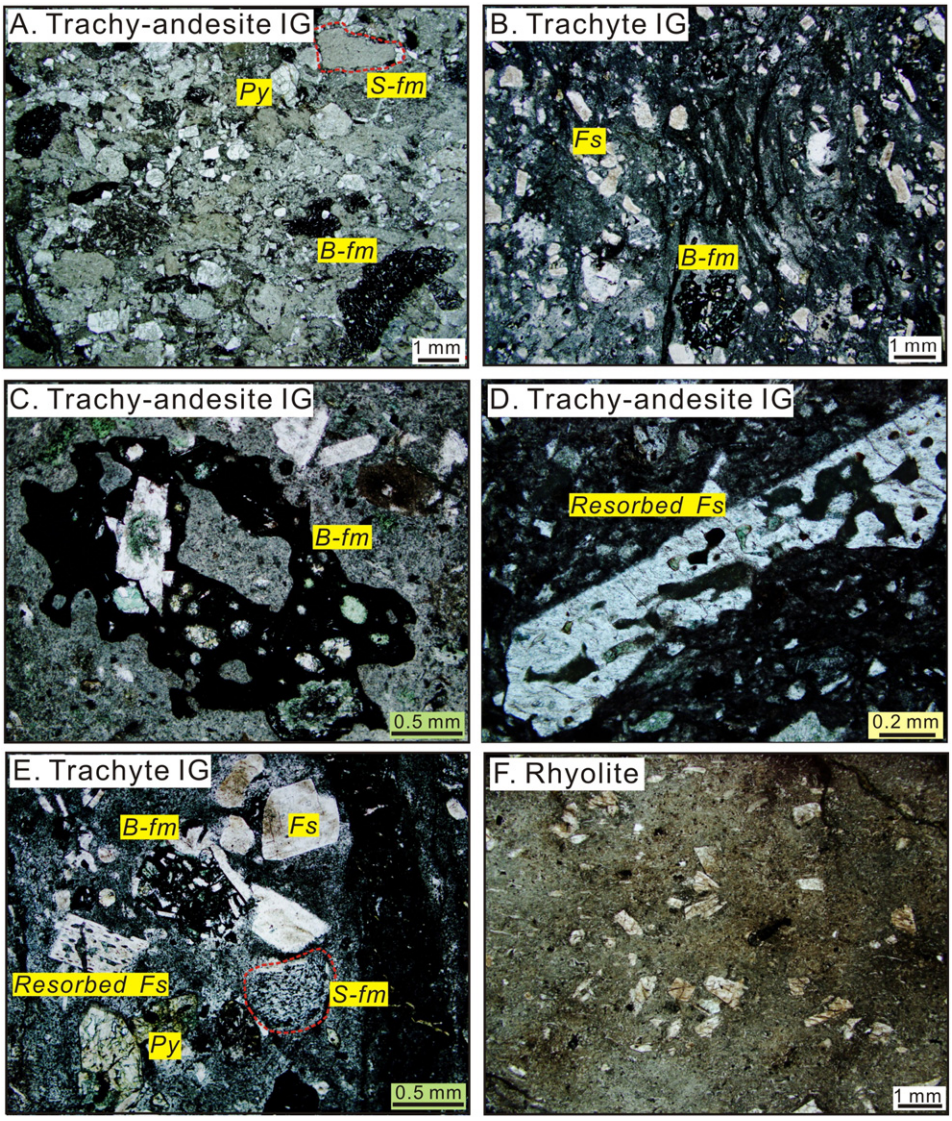

Fig. 4. Photomicrographs showing the typical textures of the trachy-andesite–trachyte ignimbrites (IG) and rhyolite lavas. Py = pyroxene; Fs = Feldspar; B/S-fm = Basaltic/Silicic fiamme. The basaltic fiammes (B-Fm) are globules-like.

Nd and Pb isotopic ratios were measured with a Micromass Isoprobe Multi-Collector ICPMS and a VG-354 mass-spectrometer at GIGCAS, respectively. The mass fractionation corrections for the Nd isotopic ratios are based on $^{146}Nd/^{144}Nd = 0.7219$. The reported $^{143}Nd/^{144}Nd$ ratios were respectively adjusted to the Shin Etsu JNdi-1 standard $^{143}Nd/^{144}Nd = 0.512115$. Repeated Pb isotopic analyses of SRM 981 yielded average values of $^{206}Pb/^{204}Pb = 16.9325 \pm 3$ (2σ), $^{207}Pb/^{204}Pb = 15.4853 \pm 3$ (2σ) and $^{208}Pb/^{204}Pb = 36.6780 \pm 9$ (2σ). External precisions are estimated to be less than 0.005, 0.005 and 0.0015.

Mineral chemistry analyses were carried out using a JEOL JXA-8230 electron probe microanalyzer (EPMA) at the GIGCAS. The operating conditions for feldspar are: 15 kV accelerating voltage, 20 nA beam current and 1 μm beam diameter. Details of these analytical methods were described by Xie et al. (2016b).

4. Results

Intermediate ignimbrites of the Liushugou Formation have LOI contents ranging from 0.7 to 2.6% and rhyolites have lower LOI contents of 0.5 to 1%. In the following plots and discussion, all oxide contents of the samples have been recalculated to 100% on a volatile-free basis with all Fe as Fe_2O_3 (Appendix A1). The Chemical Index of Alteration [CIA; $CIA = Al_2O_3 * 100 / (Al_2O_3 + CaO + Na_2O + K_2O - 3.3333 * P_2O_5)$, molar ratio] has been frequently used to study the weathering or metamorphic intensity of the rocks (Nesbitt and Young, 1982; Fedo et al., 1995; Nesbitt and Markovics, 1997). The results indicate that all the samples have CIA of 48–56, identical to the value for fresh feldspathic and granitic rocks (45 to 55), indicating that they suffered minor weathering or metamorphism.

On the classification diagram of Le Maitre (1989), the volcanics are mainly sub-alkaline and can be mainly classified as trachy-andesite, trachyte and rhyolite (Fig. 5A). Some samples are plotted in the boundary area of trachyte and dacite field and denoted as trachyte for simplicity. All samples have high alkaline contents, however, they have K_2O/Na_2O ratios are less than 1 with three exceptions of *TC-10*, *TC-23* and *DST-05*, indicating that they are predominantly sodic in composition. All but four samples (*TC-11*, *TC-18*, *TC-23*, *DST-07*) are metaluminous–slightly peraluminous with aluminium saturation index (A/CNK) <1.1 (Fig. 5B).

The trachy-andesite–trachyte ignimbrites and HAB have a linear trend of major oxides (Fig. 6) and identical trace element patterns

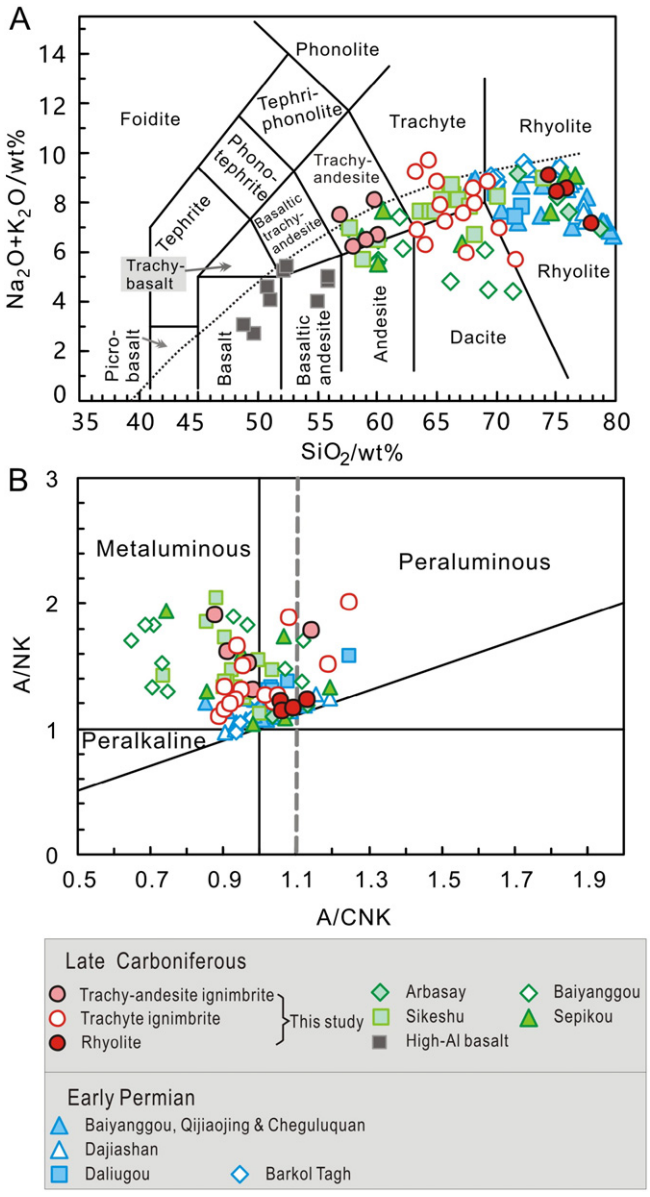

Fig. 5. (A) Total alkalis vs. Silica diagram (TAS, Le Maitre, 1989). (B) A/NK versus A/CNK. Data of the Bogda high-Al basalts (HAB) coexisted with the felsic rocks are from Xie et al. (2016b). References for the Late Carboniferous and Early Permian felsic rocks in the Bogda–Harlik belt, the north margin of Chinese North Tianshan are listed in Table 1.

(Fig. 7A and B). They have fractionated LREE/HREE with $(La/Yb)_N$ of 2.1–8.0 and $(Dy/Yb)_N$ of 1.0–2.2 and weak negative Eu anomalies with δEu of 0.73–0.97 except one high outlier ($\delta Eu_{TC\text{-}08} = 1.1$) on the chondrite-normalized REE patterns. They are also enriched in large ion lithophile elements (LILE) relative to high field-strength elements (HFSE) with very negative Nb–Ta and Ti anomalies and positive Pb anomalies, similar to arc-like affinity and distinct from ocean island basalts (OIB). The rhyolites have similar trace element feature to ignimbrites, however, they show higher $(La/Yb)_N$ and $(Dy/Yb)_N$ ratios and more negative Eu anomalies, Ti and Sr anomalies (δEu = 0.49–0.58; Fig. 7C and D).

The measured Nd and Pb isotopic ratios of the volcanics were corrected to 315 Ma based on Sm, Nd, U, Th and Pb concentrations determined by ICP–MS (Table 2). The rocks have positive $\varepsilon_{Nd(t)}$ values of >6 with young one-stage Sm–Nd model ages (T_{DM} = 504–651 Ma). Note that the Bogda intermediate ignimbrites have $\varepsilon_{Nd(t)}$ values ranging from +6.7 to +7.4, higher than that for the rhyolites ($\varepsilon_{Nd(t)}$ = +6.2 to +6.8), but similar to that of the associated HABs (Fig. 8A). The intermediate ignimbrites have $(^{206}Pb/^{204}Pb)_t$ of 17.82 to 17.89, $(^{207}Pb/^{204}Pb)_t$ of 15.48 to 15.49 and $(^{208}Pb/^{204}Pb)_t$ of 37.49 to 37.70, also similar to those for the HAB (Fig. 8C and D). In contrast, the rhyolites have relatively scattered and high $(^{206}Pb/^{204}Pb)_t$ of 17.83 to 18.05.

The trachy-andesite ignimbrites mainly contain plagioclase ($An_{30-58}Ab_{41-67}Or_{0.6-4.6}$) with minor albite (Fig. 9 and Appendix A2). The trachyte ignimbrites contain feldspars with compositions ranging from albite to plagioclases ($An_{1-61}Ab_{37-98}Or_{0.2-6.9}$), and minor K-feldspars. The highest-An plagioclase (An = 61) occurs in the trachyte ignimbrites. The rhyolites mainly contain albite and K-feldspars without plagioclase.

5. Petrogenesis of the felsic volcanics

The aluminium saturation index (A/CNK) and A/NK are indicator of the origin of granitoids (Barbarin, 1999), i.e., metaluminous and peraluminous granitoids may have incorporated crustal component in source rocks, whereas peralkaline granitoids receive a contribution from mantle materials. The source rocks of I- (A/CNK < 1.1) and S-type (A/CNK > 1.1) granitoids are generally mafic and sedimentary rocks, respectively (e.g., Chappell and White, 1992). Most of the Late Carboniferous felsic volcanics in the Bogda region are metaluminous to slightly peraluminous with A/CNK < 1.1 (Fig. 5B). Combined with their high and positive $\varepsilon_{Nd(t)}$ values (+6.2 to +7.4), indicating that the Bogda felsic volcanics belongs to I-type affinity with the contribution of juvenile crust. The origin of these felsic volcanics has been debated (e.g., Eichelberger et al., 2000; Sumner and Wolff, 2003; Dreher et al., 2005). In the following section, several possible mechanisms are discussed for the origin of the Late Carboniferous felsic volcanics in the Bogda region.

5.1. Fractional crystallization of coexisted high-Al basalt

In the binary diagrams of major oxides (Fig. 6), the felsic volcanics and HAB show similar trends of fractional crystallization. We model the fractionation history of the HAB using MELTS (Ghiorso and Sack, 1995). Variable pressures and oxygen fugacity with constant water content of 1.95 wt% and a starting composition TC-27 (Xie et al., 2016b) with the highest $\varepsilon_{Nd(t)}$ value of +7.4 are used in the modeling. The modeling results indicate that the lower pressure and/or higher oxygen fugacity could extend the fractional crystallization of the HAB more closely to rhyolite composition, but cannot generate the melts with major element compositions identical to the Bogda felsic volcanics (Fig. 6). The HAB have Zr concentrations up to 217 ppm, similar to most silicic rocks (Zr up to 206 ppm), however, the HAB have Th/Zr, Nb/Zr and U/Zr ratios remarkably different from the rhyolites (Fig. 10). In addition, the rhyolites have relatively lower $\varepsilon_{Nd(t)}$ and higher $(^{206}Pb/^{204}Pb)_t$ than HAB.

Fractionation of basaltic magmas or partial melting of mafic rocks will produce small amounts of silicic magma (Knesel and Davidson, 1997; Peccerillo et al., 2003). 10 km^3 of parental basaltic equivalents are required to generate 1 km^3 of rhyolite. The relative proportion of the basaltic and felsic rocks of the Liushugou Formation is not in agreement with this mass-balance consideration. All these lines of evidence are against the fractional crystallization of the HAB as the principle process to form the Bogda felsic rocks.

5.2. Crustal melting

Partial melting modeling requires a hydrated basaltic crust or the presence of extra heat (Pin and Paquette, 1997). However, extra heat input is inconsistent with low zircon saturation temperatures (T_{Zr} = 734–817 °C) recorded by the felsic volcanics in this study (Appendix A1). A number of melting experiments have been conducted

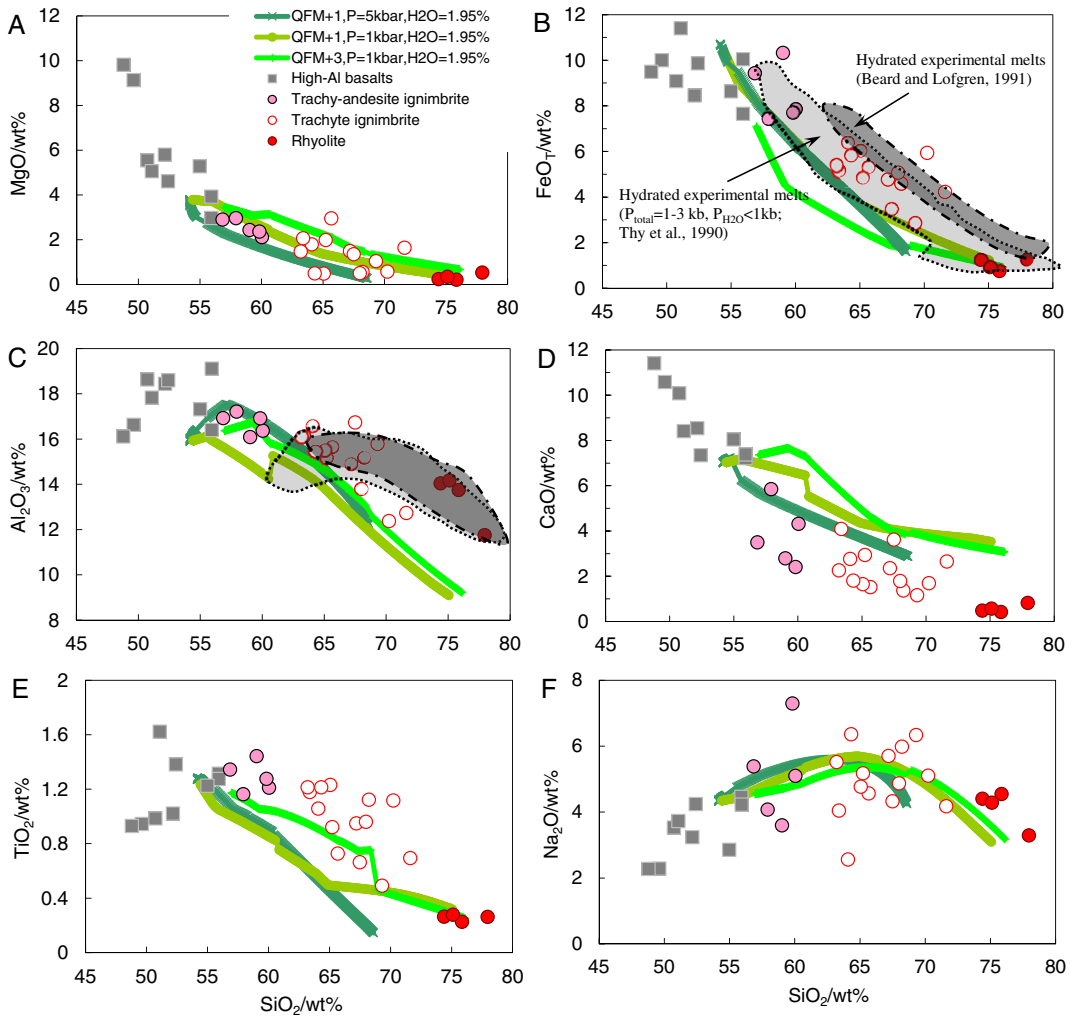

Fig. 6. Binary diagrams of major oxides versus SiO_2. Data of the Bogda high-Al basalts (HAB) coexisted with the felsic rocks are from Xie et al. (2016b). "QFM" is the abbreviation of the quartz–fayalite–magnetite oxygen buffer. The curves are the liquid curves calculated by MELTS program under different conditions. The shadow fields are after previous experimental melts of hydrated basaltic crust (Thy et al., 1990; Beard and Lofgren, 1991).

on natural and synthetic basaltic systems in different hydrated conditions over the pressure range of 1 atm to 10 kbar (Helz, 1978; Conrad et al., 1988; Ellis and Thompson, 1988; Thy et al., 1990; Beard and Lofgren, 1991). These experimental results indicate that water pressure plays a key role on the compositions of melts, whereas oxygen fugacity and compositions of starting materials also functioned in the process. The Bogda felsic volcanics have FeO_T and Al_2O_3 contents scattered within the compositional range of experimental melts of hydrated basaltic crust (Fig. 6B, C), supporting that the Bogda felsic volcanic rocks are dominantly formed by partial melting of a hydrated mafic crust. Unlike melting–mingling texture in intermediate ignimbrites (see discussion below), the rhyolites show a porphyritic texture. This suggests that the compositions of rhyolites are further close to the primitive magma produced by partial melting of a hydrated mafic crust than the ignimbrites. As the rhyolites have arc-like trace element and high Nd isotopic compositions, we therefore consider that they may have derived from a juvenile arc crust. The Bogda rhyolites have very negative Eu, Ti and Sr anomalies (Fig. 7C and D), consistent with fractionation of feldspar and Fe–Ti oxides. In fact, Thy et al. (1990) proposed that the residual phase of partial melting in a water-poor system will be plagioclase-rich with magnetite, ilmenite and apatite. Results of a dehydration-melting experiment indicate that about 50% plagioclase and magnetite and ilmenite were left in the residue phase (Beard and Lofgren, 1991). We thus prefer that the negative Eu, Sr and Ti anomalies and low Sr/Y ratios of the Bogda rhyolites are probably related to the presence of plagioclase and Fe–Ti oxides in the residue phase.

5.3. Extensive magma mingling and feldspar fractionation processes

In the trachy-andesite–trachyte ignimbrites, the heterogeneous matrix is usually composed of feldspar microlite and black glass, or tiny feldspathic minerals, and the basaltic and silicic fiammes coexist within the ignimbrites (Fig. 4). Furthermore, the globule-like basaltic fiammes are mostly sub-spherical with lobate or crenulated margins, indicating that the basaltic liquid was molten and became cooled when it was in contact with a cooler silicic magma before eruption (Blundy and Sparks, 1992; Freundt and Schmincke, 1992; Sumner and Wolff, 2003). Many feldspar fragments display irregular or resorbed shapes with embayed margins, indicating chemical disequilibrium between feldspar and liquid (Fig. 4D, E; Troll and Schmincke, 2002; Sumner and Wolff, 2003). Moreover, feldspars in the ignimbrites show a very large compositional range (Fig. 9). The highest-An plagioclase (An = 61) occurs in the trachyte rather than trachy-andesite ignimbrites. These features indicate that magma mingling between the HAB and rhyolite has also played an important role in the evolution of the Bogda intermediate ignimbrites.

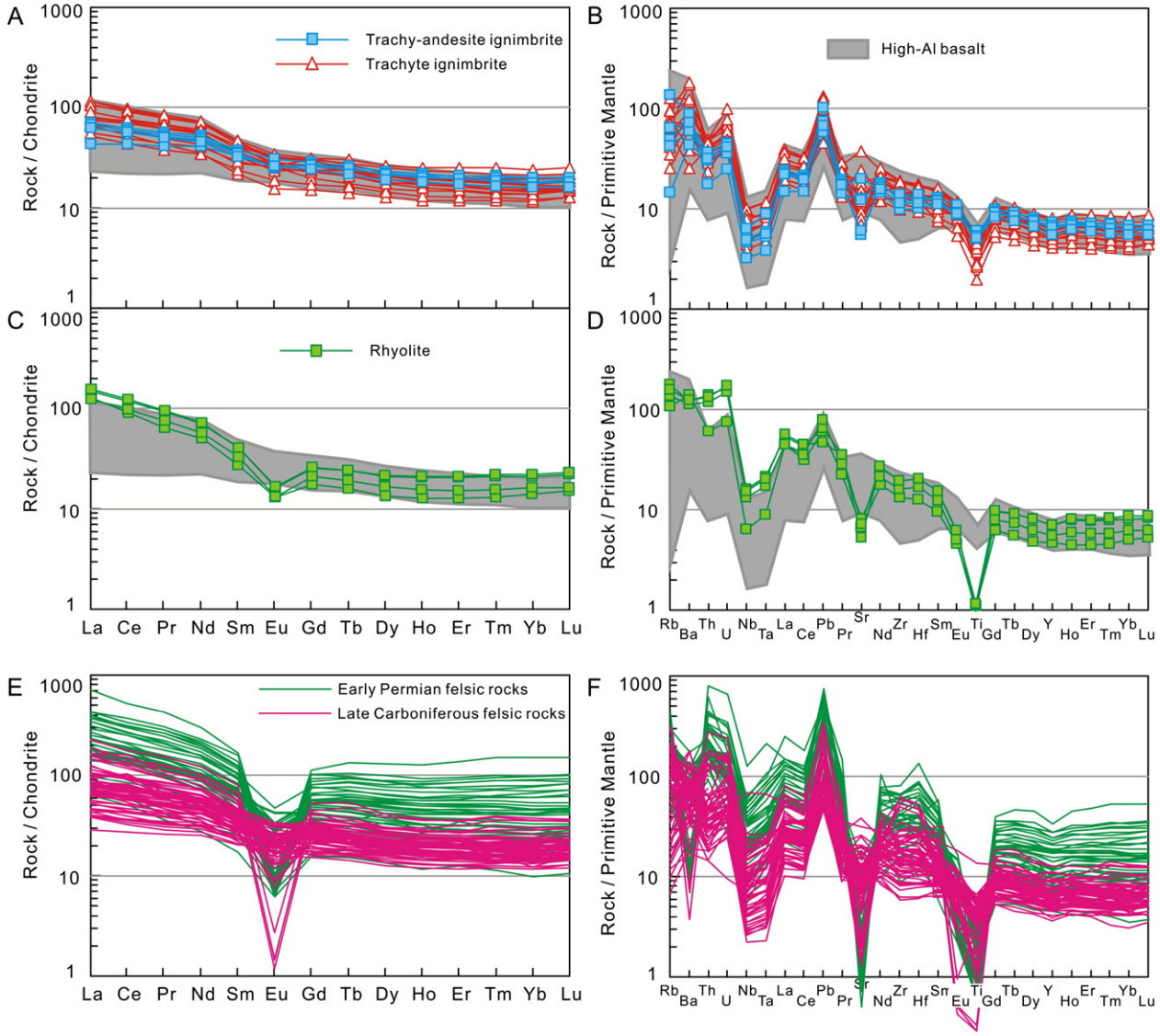

Fig. 7. Chondrite-normalized REE diagrams (A, C, E) and primitive mantle-normalized multi-element variation diagrams (B, D, F) for the Bogda–Harlik felsic rocks. Normalizing values are cited from Sun and McDonough (1989). Figs. E, F are shown for comparing the Late Carboniferous and Early Permian felsic rocks in the Bogda–Harlik belt.
Data sources are listed in Table 1.

Abundant feldspar aggregates (Fig. 4E) with various δEu ratios (Fig. 10D) indicate that the parental magma of the Bogda felsic rocks experienced feldspar fractionation and accumulation. The assimilation–fractional crystallization (AFC) modeling by DePaolo (1981) is applied to constrain the fractionation process. The HAB sample TC-27 (Xie et al., 2016b) with the highest $\varepsilon_{Nd(t)}$ and δEu = 1 and the rhyolite sample DST-05 with the highest Zr concentration and low $\varepsilon_{Nd(t)}$ are selected as two end-members (Table 3). The results show that the intermediate ignimbrites could be well produced by AFC modeling from a single starting composition with different *r* values (the ratio of the assimilation rate to the fractional crystallization rate; Fig. 10). This is further supported by the Nd and Pb isotopes, i.e., $\varepsilon_{Nd(t)}$ and $(^{206}Pb/^{204}Pb)_t$ increase with the increase of Sm/Nd and SiO_2, respectively (Fig. 8A and B).

6. Tectonic implication

The Bogda–(Harlik) belt, as the northern margin of the Chinese North Tianshan, is an important tectonic belt and recorded Phanerozoic, especially Carboniferous–Permian, crustal growth of the CAOB (Sengör et al., 1993; Jahn et al., 2000; Xiao et al., 2004; Windley et al., 2007; Safonova et al., 2011; Wilhem et al., 2012; Xiao et al., 2013). Surrounding the Junggar Basin, numerous ophiolites are exposed in East and West Junggar terranes, East Kazakhstan and North Tianshan. These terranes can be appropriately referred to "Carboniferous island-arc assemblages" (Tang et al., 2012; Kurganskaya et al., 2014; Yang et al., 2014; Jiang et al., 2015; D. Li et al., 2015; Yang et al., 2015), and no rocks of Precambrian age have been documented (Coleman, 1989; Hu et al., 2000). These ophiolites emplaced during 325–531 Ma (zircon U–Pb ages) with positive $\varepsilon_{Nd(t)}$ values (+5 to +9) (Xu et al., 2013 and references therein). Among them, the Kelameili and Bayinggou ophiolites nearby the Bogda belt (Fig. 1) are two youngest ophiolites with emplacement ages of 325 and 347 Ma (Jian et al., 2005; Xu et al., 2006a, 2006b; Wang et al., 2009, 2015). They probably represent remnants of Paleo-Tianshan Ocean (Xiao et al., 2004, 2008; Han et al., 2010).

The tectonic evolution in the Bogda Belt and even the whole Tianshan Orogen during the Carboniferous–Permian still remains debated. The Permian Tarim Plume was considered to have extended to the western Tarim Basin (e.g., Yang et al., 2007; Zhang et al., 2008;

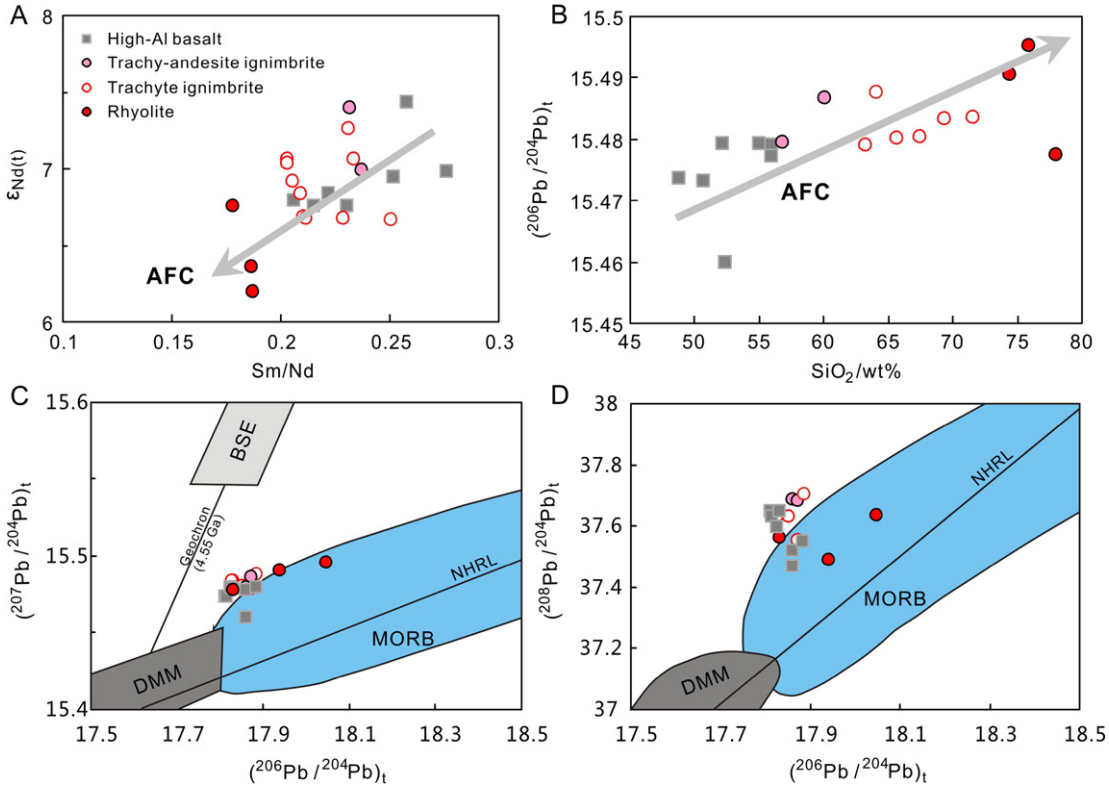

Fig. 8. (A, B) Plots of $\varepsilon_{Nd(t)}$ versus Sm/Nd and $(^{206}Pb/^{204}Pb)_t$ versus SiO_2, showing the effect of assimilation–fractional crystallization (AFC). (C, D) Plots of initial Pb isotopic compositions. The Northern Hemisphere Reference Line (NHRL, Hart, 1984) and mantle end-members (Zindler and Hart, 1986) are also shown for comparison. BSE, bulk silicate Earth; MORB, mid-ocean ridge basalt; and DMM, depleted MORB mantle.
Data source is same as in Fig. 6.

Zhou et al., 2009; Xu et al., 2014) and may affect the Tianshan Orogen, which may explain the extensive Early Permian thermal anomalies and high-temperature A_2-type granitoids and Cu–Ni-bearing mafic–ultramafic intrusion in this region (e.g., Pirajno et al., 2008; Qin et al., 2011; Liu et al., 2013; Zhang and Zou, 2013). ~300 Ma kimberlitic intrusions (Zhang et al., 2013) and Fe–Ti oxide-bearing mafic layered intrusion (He et al., 2016) in the southwest part of the Tianshan Orogen was attributed to the beginning of the Tarim Plume at the end of Carboniferous (Zhang et al., 2013; Xu et al., 2014; He et al., 2016). Devonian OIB-like mafic magmatism and ocean plate stratigraphy might even imply that the plume magmatism was active in the southern Tianshan Ocean in Devonian (Safonova et al., 2016). In the Bogda region, a Carboniferous–Permian continental rift associated with a mantle plume model is also suggested mainly based on the Carboniferous bimodal volcanism (Gu et al., 2000, 2001; Xia et al., 2008, 2012). However, these are not robust evidence for a mantle plume model. Occurrence of bimodal volcanism just implies an extensional environment rather than being exclusively associated with a continental rift. OIB-like or picritic magmatism related to a mantle plume has not yet found in this region. In this study, the volcanics of the Upper Carboniferous Liushugou Formation are not bimodal in composition, but their generation is related to bimodal magma (basaltic and rhyolitic magmas), indicating an extensional environment. Occurrence of the Bogda high-Al basalt (HAB) and pillow basalt suggests a back-arc (or rear-arc) setting for the Bogda belt in the Late Carboniferous (Xie et al., 2016a, 2016b). Therefore, an alternative setting for the Bogda belt is that it was a back-arc extensional environment in the Carboniferous (Fig. 13A) (Chen et al., 2013; Zhang et al., 2016; Xie et al., 2016a, 2016b).

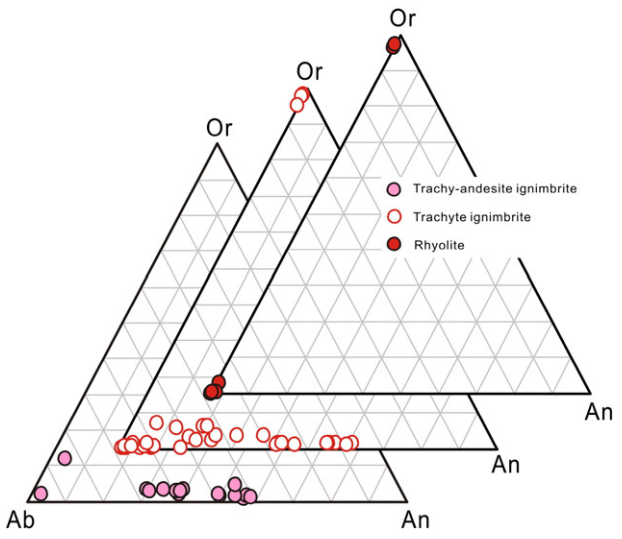

Fig. 9. Normative An–Ab–Or for plagioclase (Pl) from the Bogda felsic rocks.

The Bogda–Harlik island arc was considered to have formed in Devonian–Carboniferous due to the southward subduction of the Kelameili Ocean (Ma et al., 1997; Xiao et al., 2004; Sun et al., 2005; Yuan et al., 2010). The arc is mainly composed of Ordovician to Silurian marine clastic rock and tuff, interlayered with limestone and subordinate basalt (Huangcaopo Group; Ma, 1999). It eventually developed to a mature arc in the Devonian and Carboniferous and is composed of Devonian–Carboniferous mafic and felsic volcanic rocks (Ma et al., 1997; Xiao et al., 2004). Han et al. (2010) documented a ca. 316 Ma "stitching pluton" which intruded the Bayingou ophiolites and argued that the "stitching pluton" is likely of post-collisional A-type granites.

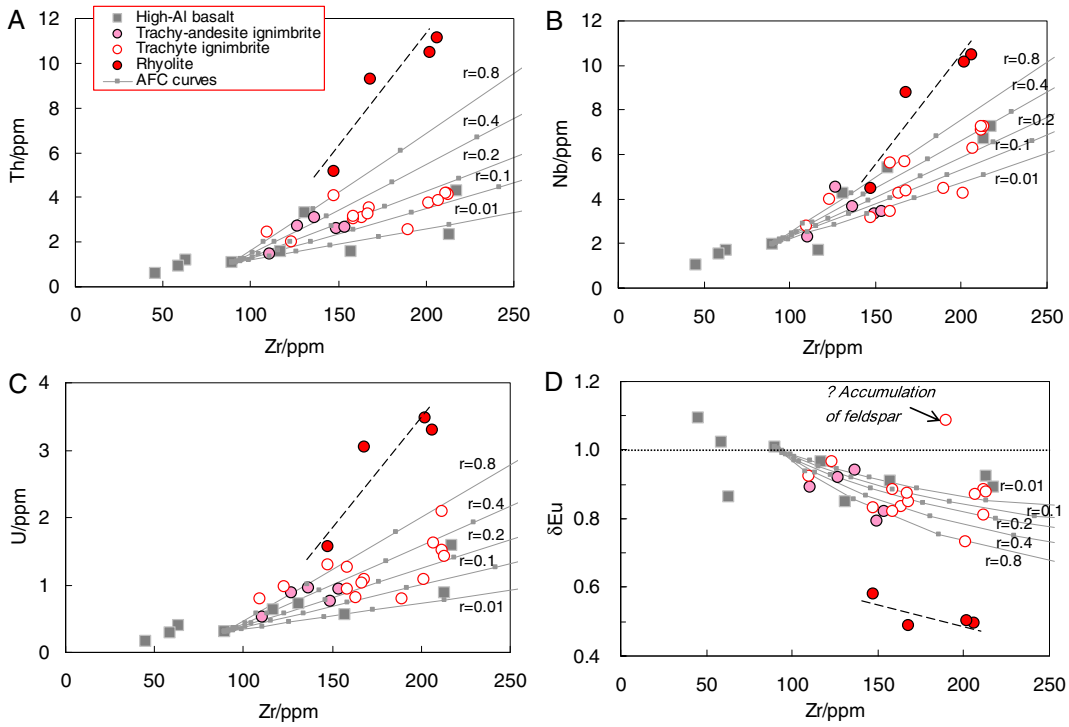

Fig. 10. Plots of Th, Nb, U and δEu versus Zr of the Bogda felsic rocks. The calculated solid curves represent assimilation–fractional crystallization trends (AFC; DePaolo, 1981) with ticks at 10% increments of crystallization. The parameters for calculation are listed in Table 3.
Data source is same as in Fig. 6.

The closure of the Paleo-Tianshan Ocean is therefore considered to be at the end of Early Carboniferous followed by a post-collisional orogenic setting (Han et al., 2010; Chen et al., 2011; Han et al., 2011). However, this "stitching pluton" has SiO_2 contents highly variable from 58 to 74 wt%), consistent with metaluminous I-type affinity rather than typical A-type (Figs. 5, 11) (Si et al., 2014). The calculated zircon saturation temperatures (T_{Zr} = 792–842 °C) were also in the overlapped field of typical A-type and I-type granitoids (King et al., 1997; Zhong and Xu, 2009; Liu et al., 2013). In fact, the Late Carboniferous felsic rocks in the Chinese Tianshan Orogenic Belts often belong to I-type (Zhu et al., 2009; Tang et al., 2010; Tong et al., 2010; Liu et al., 2013; Tang et al., 2014; Zhang et al., 2015), whereas the Early Permian felsic rocks are mainly A-type granitoids (Tang et al., 2010; Yuan et al., 2010; Zhang and Zou, 2013; N.-B. Li et al., 2015). Therefore, we assume an island arc system in the Bogda belt in association with southward subduction of the Paleo-Tianshan Ocean during Devonian–Carboniferous and a post-collisional extensional environment in the Permian (Ma et al., 1997; Laurent-Charvet et al., 2003; Xiao et al., 2004; Yuan et al., 2010; Chen et al., 2011).

In the Bogda region, the Carboniferous strata are characterized by marine to shallow-marine sedimentary and volcanic rocks, whereas the Permian strata are mainly composed of terrestrial sediments with volcanic lavas. Pillow lavas and the late Carboniferous marine Echinodermata fossil occur in the Qijiagou Formation (Xie et al., 2016a). The Early Permian terrestrial charred wood of *Prototaxoxylon* was documented in the Wutonggou Formation (Wan et al., 2016). The change of paleogeographic environment mirrored the transition from marine to continental environment during Carboniferous–Permian (Carroll et al., 1990; Wartes et al., 2002; Obrist-Farner and Yang, 2015). Together with occurrence of thick red molasse along the south margin of the Bogda belt and the large-scale strike–slip shearing and rifting in the Early Permian (Shu et al., 2005), we suggest that an important tectonic transformation occurred between Carboniferous and Permian in the Bogda belt.

Granitic and volcanic systems have inherently different cooling rates, but the compositional similarities of intrusive and extrusive rocks may record similar magmatic processes and unravel the origin (Pearce et al., 1984). Such magma-mingling ignimbrite samples cannot represent the compositions of primary magma or residual melt. Thus, we just use the rhyolites to discuss tectonic implication. Zircon saturation temperature is a useful parameter in petrogenetic evaluation. The combined geological and geochemical approaches represent a simple and powerful way to illuminate important issues of magma genesis, and then to define their tectonic setting (e.g., Watson and Harrison, 1983; Miller et al., 2003; Liu et al., 2013). We collected and compared the Late Carboniferous–Early Permian felsic rocks with reliable zircon U–Pb ages in this region (see Table 1 and Fig. 5). The Late Carboniferous felsic rocks, with exception of the Sepikou rhyolite (Gao et al., 2013), have relatively low zircon saturation temperatures (T_{Zr} = 706–842 °C; Fig. 12B), and are mostly I-type granitoids in arc settings (Fig. 11). Those with $\varepsilon_{Nd(t)}$ values of +5.9 to +7.5 (Fig. 12A) and young one-stage Sm–Nd model ages indicate that the Bogda belt was also essentially built up by juvenile arc crust in the Late Carboniferous (e.g., Jahn et al., 2000).

Compared with the subduction-related magmatism in the Late Carboniferous, magmatism in the Early Permian is mainly bimodal volcanism (293–297 Ma), including A_2-type granites (284–288 Ma) and coeval mafic dykes/intrusions. Unlike the Late Carboniferous felsic rocks, the Early Permian felsic rocks in the Bogda belt have much higher REE and incompatible elements (Fig. 7E and F) and lower $\varepsilon_{Nd(t)}$ values of +1.9 to +6.0 (Fig. 12A), typical of within-plate felsic rocks (Fig. 11). Furthermore, the Early Permian felsic rocks show relatively high zircon saturation temperatures (T_{Zr} = 841–956 °C; Fig. 12B), similar to those of A-type granitoids (T_{Zr} > 800 °C) from the Lachlan Fold Belt (King et al., 1997), Tarim LIP (Liu et al., 2014) and other tectonic terranes in NW China (Liu et al., 2013). The temporal geochemical shift and thermal anomaly from Late Carboniferous to Early Permian are likely related to mantle-derived magma upwelling, either as a

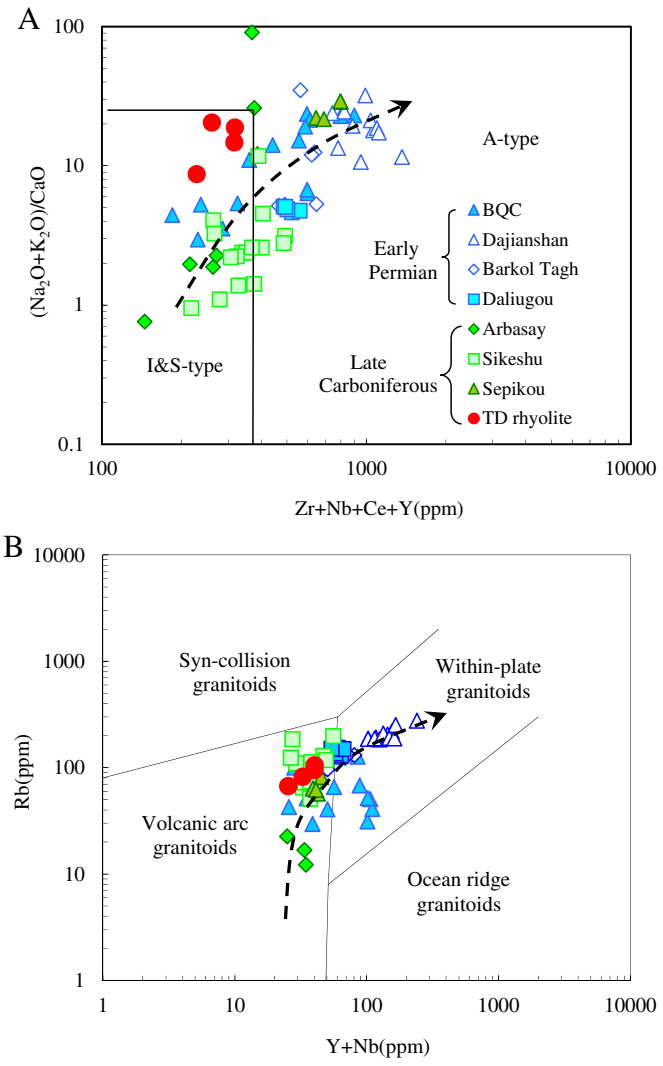

Fig. 11. (A) ($Na_2O + K_2O$) / CaO versus Zr + Nb + Ce + Y (Whalen et al., 1987). (B) Rb versus Y + Nb (Pearce et al., 1984). BQC and TD are short for Baiyanggou, Qijiajing & Cheguluquan and Tianchi & Dashitou, respectively.

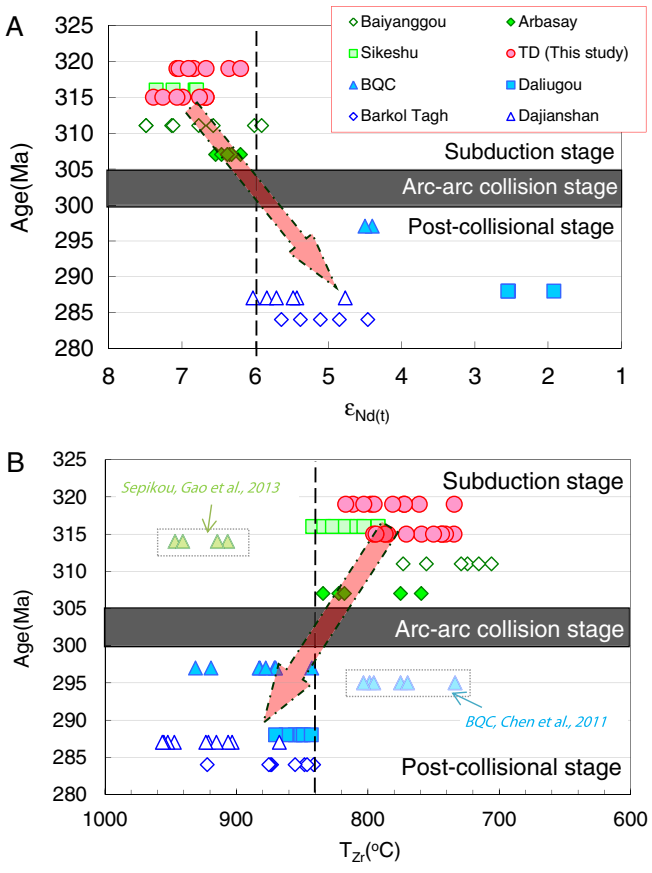

Fig. 12. Plots of $\varepsilon_{Nd(t)}$ (A) and zircon saturation temperature (B) versus ages of the felsic rocks at the north margin of the Chinese North Tianshan. BQC and TD are short for Baiyanggou, Qijiajing & Cheguluquan and Tianchi & Dashitou, respectively.

result of post-collisional lithospheric collapse (e.g., Yuan et al., 2010) or driven by mantle plume (e.g., Pirajno et al., 2008; Liu et al., 2013). We prefer that the Paleo-Tianshan Ocean around the Bogda region likely terminated at the end of Late Carboniferous. In the Early Permian, the Bogda belt was possibly a post-collisional setting which may have witnessed "soft" arc–arc collision (Fig. 13B) (East Junggar arc vs. Bogda arc; Ma et al., 1997; Xiao et al., 2004; Yuan et al., 2010; Shu et al., 2011; Wilhem et al., 2012; Xiao et al., 2013; Xie et al., 2016a). The collision between the East Junggar and Bogda arcs is similar to the collision of Halmahera and Sangihe arcs in SE Asia and SW Pacific (e.g., Hall, 1996; Charlton, 2000) and the collision of Wallowa and Olds Ferry arc in the western North America

Table 1
Brief introduction of the Late Carboniferous–Early Permian felsic rocks with zircon U–Pb ages in the Bogda-Harlik belt, the north margin of Chinese North Tianshan.

Number	Location	Rock	Age/Ma	Method	References
1	Arbasay	Rhyolite–dacite–andesite–basaltic lava with felsic ignimbrite	307 ± 1.3	SHRIMP	Liu et al. (2012)
			314 ± 3.4	LA-ICP-MS	Liu et al. (2015)
2	Sikeshu	Diorite–granodiorite–granite ("*stitching*" *pluton*)	316 ± 2.5	SHRIMP	Han et al. (2010)
					Si et al. (2014)
3	Tianchi (N43°54.5′ E88°7′)	Rhyolite–trachyte–trachy-andesite ignimbrite with high-Al basaltic lava	315 ± 2	SHRIMP	Xie et al. (2016b)
					This study
4	Baiyanggou (N43°41′ E88°3′)	Rhyolite–dacite–andesite ignimbrite with pillow basaltic lava	311 ± 2	SHRIMP	Xie et al. (2016a)
					Our unpublished data
5	Baiyanggou	Rhyolite–basalt bimodal lava	293 ± 1.7	LA-ICP-MS	Chen et al. (2011)
6	Dashitou (N43°44′ E91°10′)	Rhyolite–trachyte–trachy-andesite ignimbrite with high-Al basaltic lava	319 ± 3	SHRIMP	Xie et al. (2016b)
					This study
7	Sepikou	Rhyolite	314 ± 1.1	LA-ICP-MS	Gao et al. (2013)
8	Qijiaojing	Rhyolite–basalt bimodal lava	295 ± 2	LA-ICP-MS	Chen et al. (2011)
9	Cheguluquan	Rhyolite–basalt bimodal lava	294 ± 2.3	LA-ICP-MS	Chen et al. (2011)
			297 ± 3	SHRIMP	Our unpublished data
10	Dajiashan	Monzogranite	287 ± 2	SHRIMP	Yuan et al. (2010)
11	Daliugou	Granite	288 ± 3	SHRIMP	Yuan et al. (2010)
12	Barkol Tagh	Biotite monzogranite	284 ± 5	SHRIMP	Yuan et al. (2010)
13	Baishitou	Diorite	316 ± 3	SHRIMP	Sun et al. (2005)

Table 2
Whole rock Nd and Pb isotopic compositions of the Bogda felsic volcanics.

Sample	TC-07	TC-16	TC-04	TC-08	TC-11	TC-15	TC-23	DST-02	DST-09	DST-10	DST-13	DST-14	TC-10	DST-05	DST-06
Rock	Trachy-andesite ignimbrite		Trachyte ignimbrite										Rhyolite lava		
Nd	24.4	23.5	16.0	19.9	21.5	16.5	26.8	19.1	34.4	34.2	28.1	32.7	23.3	33.0	26.9
Sm	5.78	5.46	3.66	4.18	4.98	3.35	6.72	4.46	6.99	7.15	5.94	6.72	4.15	6.15	5.04
Pb	7.25	4.91	4.19	3.96	7.08	3.26	9.45	4.40	6.96	6.07	5.57	9.33	4.29	9.75	11.81
Th	3.077	2.587	2.465	2.55	3.04	4.09	3.12	2.01	4.16	3.84	3.23	4.19	5.15	11.1	9.30
U	0.958	0.752	0.786	0.799	0.936	1.30	0.804	0.968	2.09	1.62	1.03	1.51	1.56	3.30	3.05
$^{143}Nd/^{144}Nd$	0.512886	0.512900	0.512860	0.512838	0.512893	0.512848	0.512887	0.512884	0.512845	0.512842	0.512836	0.512841	0.512801	0.512788	0.512781
$\pm 2\sigma$	0.000004	0.000004	0.000003	0.000003	0.000003	0.000004	0.000004	0.000004	0.000004	0.000003	0.000003	0.000006	0.000003	0.000004	0.000003
$(^{143}Nd/^{144}Nd)_i$	0.512591	0.512612	0.512575	0.512576	0.512605	0.512595	0.512574	0.512590	0.512588	0.512578	0.512569	0.512582	0.512579	0.512553	0.512545
$\varepsilon_{Nd(t)}$	6.99	7.39	6.67	6.69	7.26	7.07	6.67	7.07	7.04	6.84	6.67	6.91	6.76	6.36	6.20
T_{DM} (Ma)	576	521	590	554	534	510	651	562	516	542	561	529	504	548	562
$^{206}Pb/^{204}Pb$	18.28	18.36	18.41	18.46	18.27	19.11	18.15	18.57	18.59	18.63	18.38	18.39	19.00	19.04	18.88
$\pm 2\sigma$	0.03	0.03	0.04	0.03	0.03	0.05	0.03	0.04	0.03	0.03	0.03	0.03	0.03	0.03	0.03
$^{207}Pb/^{204}Pb$	15.50	15.51	15.51	15.51	15.50	15.55	15.50	15.52	15.50	15.50	15.49	15.49	15.54	15.55	15.54
$\pm 2\sigma$	0.03	0.03	0.03	0.03	0.03	0.04	0.03	0.03	0.02	0.03	0.03	0.03	0.03	0.03	0.03
$^{208}Pb/^{204}Pb$	38.12	38.22	38.24	38.29	38.07	38.95	38.04	38.02	38.06	38.13	38.05	37.94	38.81	38.69	38.46
$\pm 2\sigma$	0.11	0.17	0.14	0.1	0.11	0.16	0.12	0.12	0.12	0.12	0.14	0.12	0.13	0.12	0.12
$(^{206}Pb/^{204}Pb)_i$	17.86	17.87	17.83	17.82	17.85	17.83	17.89	17.87	17.63	17.77	17.79	17.87	17.83	17.94	18.05
$(^{207}Pb/^{204}Pb)_i$	15.48	15.49	15.48	15.48	15.48	15.48	15.49	15.48	15.45	15.46	15.46	15.46	15.48	15.49	15.50
$(^{208}Pb/^{204}Pb)_i$	37.69	37.68	37.65	37.63	37.63	37.64	37.70	37.55	37.44	37.47	37.45	37.48	37.56	37.49	37.64

Table 3
Selected two end-number samples and trace element partition coefficients for AFC model.

Sample	Nb	Zr	Th	U	Sm	Eu	Gd	$\varepsilon_{Nd(t)}$	References
TC-27	1.98	89.6	1.06	0.306	3.81	1.32	4.16	7.43	Xie et al. (2016b)
DST-05	10.5	206	11.1	3.3	6.15	0.938	5.17	6.2	This study
Partition coefficient D									
Plagioclase (75%)	0.01	0.01	0.01	0.05	0.02	0.3	0.05		GERM website
Olivine (1%)	0.01	0.01	0.0001	0.0001	0.004	0.005	0.004		(http://www.earthref.org/databases/KDD/main.htm)
Clinopyroxene (20%)	0.008	0.2	0.013	0.017	0.3	0.3	0.6		
Orthopyroxene (1%)	0.001	0.032	0.001	0.017	0.015	0.03	0.034		
Magnetite (3%)	0.07	0.7	0.1	0.1	0.026	0.025	0.018		
Bulk D	0.011	0.069	0.013	0.044	0.076	0.286	0.158		

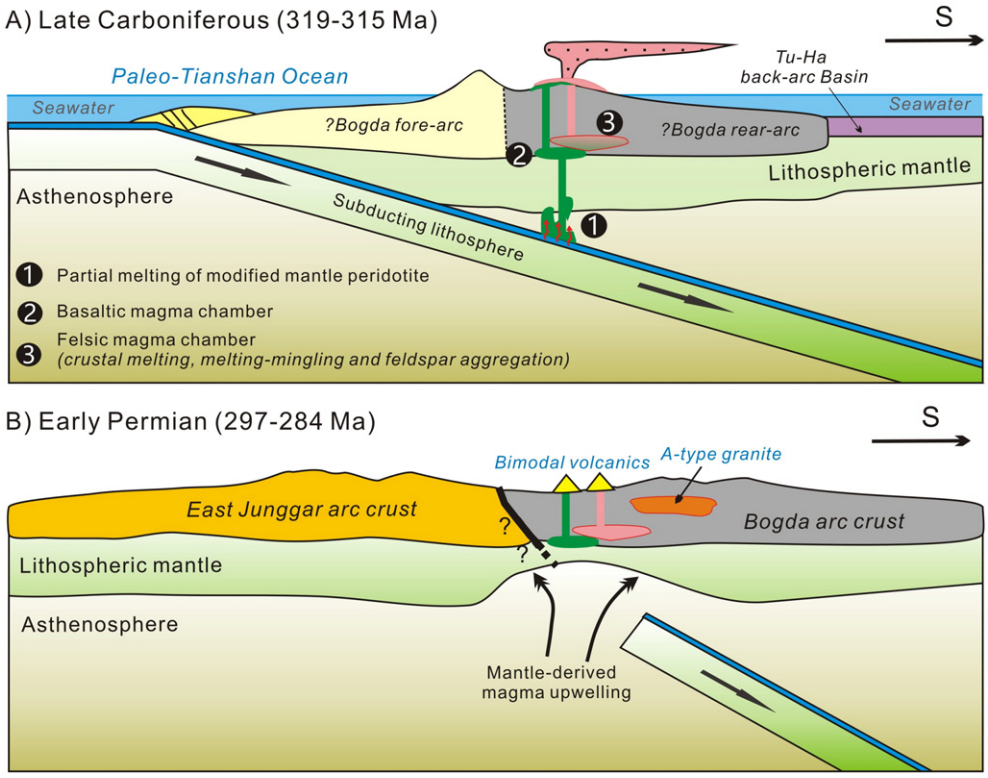

Fig. 13. Idealized illustration for the Late Carboniferous to Early Permian tectonic evolution in the Bogda belt: A) an arc system for the generation of the felsic volcanics in the Late Carboniferous; B) a post-collisional setting after "soft" arc–arc collision in the Early Permian modified after Yuan et al. (2010) and Chen et al. (2011).

(e.g., Dorsey and LaMaskin, 2007). However, such "soft" arc–arc collision may only last for a very short time (<10 Ma; Fig. 12).

7. Conclusion

The I-type felsic volcanics (315–319 Ma) of the Upper Carboniferous Liushugou Formation in the Bogda belt is in conformable contact with the high-Al basalts. They are composed of trachy-andesite–trachyte ignimbrites and rhyolite lavas and show arc-like geochemical characteristics with low zircon saturation temperatures. The Bogda intermediate ignimbrites and rhyolites mainly formed by partial melting of a juvenile and hydrated arc crust rather than by fractional crystallization of the coexisted high-Al basalts. However, melting–mingling textures, abundant feldspar aggregates and various δEu ratios are consistent with that magma mingling and feldspar fractionation processes also played an important role in the genesis of the felsic ignimbrites. We propose that the Carboniferous island arc system was followed by a post-collisional orogenic system in the Early Permian by arc–arc collision at the end of Late Carboniferous.

Supplementary data to this article can be found online at http://dx.doi.org/10.1016/j.gr.2016.07.005.

Acknowledgements

This study was funded by National Basic Research Program of China (2011CB808906), NSFC Grants (No. 41503017, 415030057 and 41203009) and China Postdoctoral Science Foundation Grant (2013M542214). The study is a contribution to IGCP#592. We are grateful to the constructive reviews of Professor Liangshu Shu and the other four anonymous reviewers and associate editor Inna Safonova. We thank Christina Yan Wang for revising the paper privately. We also thank Hang-Qiang Xie, Yin Liu, Guang-Qian Hu, Jin-Long Ma, and Chang-Ming Xing for their technical help in analyses.

References

Barbarin, B., 1999. A review of the relationships between granitoid types, their origins and their geodynamic environments. Lithos 46, 605–626.
Beard, J., Lofgren, G.E., 1991. Dehydration melting and water-saturated melting of basaltic and andesitic greenstones and amphibolites at 1, 3 and 6.9 kb. Journal of Petrology 32, 365–402.
BGMRXUAR (Bureau of Geology and Mineral Resources of Xinjiang Uygur Autonomous Region), 1993. Regional geology of Xinjiang Autonomous Region, Geological Memoirs, No. 32, Map Scale 1:500000. Geological Publishing House, Beijing (in Chinese).
Blundy, J.D., Sparks, R.S.J., 1992. Petrogenesis of mafic inclusions in granitoids of the Adamello Massif, Italy. Journal of Petrology 33, 1039–1104.
Branney, M.J., Kokelaar, B.P., 2002. Pyroclastic density currents and the sedimentation of ignimbrites. Geological Society of London's Memoirs 27 (143 pp.).
Carroll, A.R., Liang, Y., Graham, S.A., Xiao, X., Hendrix, M.S., Chu, J., McKnigth, C.L., 1990. Junggar basin, northwestern China: trapped Late Paleozoic ocean. Tectonophysics 181, 1–14.
Chappell, B.W., White, A.J.R., 1992. I- and S-type granites in the Lachlan Fold Belt. Transactions of the Royal Society of Edinburgh: Earth Sciences 83, 1–26.
Charlton, T.R., 2000. Tertiary evolution of the Eastern Indonesia collision complex. Journal of Asian Earth Sciences 18, 603–631.
Charvet, J., Shu, L.S., Laurent-Charvet, S., 2007. Paleozoic structural and geodynamic evolution of eastern Tianshan (NW China): welding of the Tarim and Junggar plates. Episodes 30, 162–186.
Charvet, J., Shu, L.S., Laurent-Charvet, S., Wang, B., Faure, M., Cluzel, D., Chen, Y., de Jong, K., 2011. Palaeozoic tectonic evolution of the Tianshan belt, NW China. Science China Earth Sciences 54, 166–184.
Chen, X., Shu, L., Santosh, M., 2011. Late Paleozoic post-collisional magmatism in the Eastern Tianshan Belt, Northwest China: new insights from geochemistry, geochronology and petrology of bimodal volcanic rocks. Lithos 127, 581–598.
Chen, X., Shu, L., Santosh, M., Zhao, X., 2013. Island arc-type bimodal magmatism in the eastern Tianshan Belt, Northwest China: geochemistry, zircon U–Pb geochronology and implications for the Paleozoic crustal evolution in Central Asia. Lithos 168–169, 48–66.
Chen, X., Shu, L., Santosh, M., Xu, Z., 2014. The provenance and tectonic affinity of the Paleozoic meta-sedimentary rocks in the Chinese Tianshan belt: new insights from detrital zircon U–Pb geochronology and Hf-isotope analysis. Journal of Asian Earth Sciences 94, 12–27.
Coleman, R.G., 1989. Continental growth of northwest China. Tectonics 8, 621–635.
Conrad, W.K., Bicholls, I.A., Wall, W.L., 1988. Water-saturated and -undersaturated melting of metaluminous and peraluminous crustal compositions at 10 kb: evidence for the origin of silicic magmas in the Taupo volcanic zone, New Zealand, and other occurrences. Journal of Petrology 29, 765–803.

Davidson, J.P., Arculus, R.J., 2006. The significance of phanerozoic arc magmatism in generating continental crust. In: Brown, M., Rushmer, T. (Eds.), Evolution and Differentiation of the Continental Crust. Cambridge Press, pp. 135–172.
DePaolo, D.J., 1981. Trace element and isotopic effects of combined wallrock assimilation and fractional crystallization. Earth and Planetary Science Letters 53, 189–202.
Dorsey, R.J., LaMaskin, T.A., 2007. Stratigraphic record of Triassic–Jurassic collisional tectonics in the Blue Mountains province, northeastern Oregon. American Journal of Science 307, 1167–1193.
Dreher, S.T., Eichelberger, J.C., Larsen, J.F., 2005. The petrology and geochemistry of the Aniakchak coldera-forming ignimbrite, Aleutian arc, Alaska. Journal of Petrology 46, 1747–1768.
Eichelberger, J.C., Chertkoff, D.G., Dreher, S.T., Nye, C.J., 2000. Magmas in collisions; rethinking chemical zonation in silicic magmas. Geology 28, 603–606.
Ellis, D.J., Thompson, A.B., 1988. Subsolidus and partial melting reactions in the quartz-excess $CaO + MgO + Al_2O_3 + SiO_2 + H_2O$ system under water-excess and water-deficient conditions to 10 kbar: some implications for the origin of peraluminous melts from mafic rocks. Journal of Petrology 27, 91–121.
Fedo, C.M., Nesbitt, H.W., Young, G.M., 1995. Unraveling the effects of potassium metasomatism in sedimentary rocks and paleosols, with implications for paleoweathering conditions and provenance. Geology 23, 921–924.
Freundt, A., Schmincke, H.-U., 1992. Mingling of rhyolite, trachyte and basalt erupted from a vertically and laterally zoned reservoir, composite flow P1, Gran Canaria. Contributions to Mineralogy and Petrology 112, 1–19.
Gao, J., Li, W., Zhou, Y., Liu, J., Fan, T., Lu, L., Zhou, R., 2013. Geochemistry, zircon U–Pb ages and geological significance of the Liushugou Formation rhyolite in the Sepikou region, eastern Bogda, Xinjiang. Geology and Exploration 49, 665–675 (in Chinese with English abstract).
Ghiorso, M.S., Sack, R.O., 1995. Chemical mass transfer in magmatic processes IV. A revised and internally consistent thermodynamic model for the interpolation and extrapolation of liquid–solid equilibria in magmatic systems at elevated temperatures and pressures. Contributions to Mineralogy and Petrology 119, 197–212.
Gu, L.X., Hu, S.X., Yu, C.S., Li, H.Y., Xiao, X.J., Yan, Z.F., 2000. Carboniferous volcanites in the Bogda orogenic belt of eastern Tianshan: their tectonic implications. Acta Petrologica Sinica 16, 305–316 (in Chinese with English abstract).
Gu, L.X., Hu, S.X., Yu, C.S., Zhao, M., Wu, C.Z., Li, H.Y., 2001. Intrusive activities during compression–extension tectonic conversion in the Bogda intracontinental orogen. Acta Petrologica Sinica 17, 187–198 (in Chinese with English abstract).
Hall, R., 1996. Reconstructing Cenozoic SE Asia. In: Hall, R., Blundell, D.J. (Eds.), Tectonic Evolution of SE Asia. Geological Society, London, Special Publications 106, pp. 153–184.
Han, B.-F., Guo, Z.-J., Zhang, Z.-C., Zhang, L., Chen, J.-F., Song, B., 2010. Age, geochemistry, and tectonic implications of a late Paleozoic stitching pluton in the North Tian Shan suture zone, western China. Geological Society of America Bulletin 122, 627–640.
Han, B.-F., He, G.-Q., Wang, X.-C., Guo, Z.-J., 2011. Late Carboniferous collision between the Tarim and Kazakhstan–Yili terranes in the western segment of the South Tian Shan Orogen, Central Asia, and implications for the Northern Xinjiang, western China. Earth-Science Reviews 109, 74–93.
Hart, S.R., 1984. A large-scale isotope anomaly in the southern hemisphere mantle. Nature 309, 753–757.
He, P.-L., Huang, X.-L., Xu, Y.-G., Li, H.-Y., Wang, X., Li, W.-X., 2016. Plume-orogenic lithosphere interaction recorded in the Haladala layered intrusion in the Southwest Tianshan Orogen, NW China. Journal of Geophysical Research - Solid Earth 121, 1525–1545.
Helz, R.Z., 1978. Phase relationships of basalts in their melting ranges at $P_{H2O} = 5$ kb. Part II, melt composition. Journal of Petrology 17, 139–193.
Hu, A.Q., Jahn, B.-m., Zhang, G., Chen, Y., Zhang, Q., 2000. Crustal evolution and Phanerozoic crustal growth in northern Xinjiang: Nd isotopic evidence. Part I. Isotopic characterization of basement rocks. Tectonophysics 328, 15–51.
Jahn, B.-m., Wu, F., Chen, B., 2000. Massive granitoid generation in Central Asia: Nd isotope evidence and implication for continental growth in the Phanerozoic. Episodes 23, 82–92.
Jian, P., Liu, D.Y., Shi, Y.R., Zhang, F.Q., 2005. SHRIMP dating of SSZ ophiolites from northern Xinjiang Province, China: implications for generation of oceanic crust in the Central Asian Orogenic Belt. In: Sklyarov, E.V. (Ed.), Structural and Tectonic Correlation Across the Central Asia Orogenic Collage: North-Eastern Segment. Guidebook and Abstract Volume of the Siberian Workshop IGCP-480. IEC SB RAS, Irkutsk, p. 246.
Jiang, Y., Xiao, L., Zhou, P., Wang, G., 2015. Geological, geochemical characteristics of Hongshan plution: constraint for lower crust of West Junggar, Xinjiang. Earth Science-Journal of China University of Geosciences 40, 1129–1147 (in Chinese with English abstract).
King, P.L., White, A.J.R., Chappell, B.W., Allen, C.M., 1997. Characterization and origin of aluminous A-type granites from the Lachlan Fold Belt, Southeastern Australia. Journal of Petrology 38, 371–391.
Knesel, K.M., Davidson, J.P., 1997. The origin and evolution of large-volume silicic magma systems: Long Valley Caldera. International Geology Review 39, 1033–1052.
Kurganskaya, E.V., Safonova, I.Y., Simonov, V.A., 2014. Geochemistry and petrogenesis of suprasubduction volcanic complexes of the Char strike-slip zone, eastern Kazakhstan. Russian Geology and Geophysics 55, 69–84.
Laurent-Charvet, S., Charvet, J., Monié, P., Shu, L., 2003. Late Paleozoic strike-slip shear zones in eastern central Asia (NW China): new structural and geochronological data. Tectonics 22, 1009–1032.
Le Maitre, R.W., 1989. A Classification of Igneous Rocks and Glossary Terms: Recommendations of the International Union of Geological Sciences Subcommission on the Systematics of Igneous Rocks. Blackwell Scientific Publications, Trowbridge, Wilts, UK, pp. 1–193.
Li, J., He, G., Xu, X., Li, H., Sun, G., Yang, T., Gao, L., Zhu, Z., 2006. Crustal tectonic framework of Northern Xinjiang and adjacent regions and its formation. Acta Geologica Sinica 80, 148–168 (in Chinese with English abstract).
Li, D., He, D., Ma, D., Tang, Y., Kong, Y., Tang, J., 2015. Carboniferous–Permian tectonic framework and its later modifications to the area from eastern Kazakhstan to southern Altai: insights from the Zaysan–Jimunai Basin evolution. Journal of Asian Earth Sciences 113, 16–35.
Li, N.-B., Niu, H.-C., Shan, Q., Yang, W.-B., 2015. Two episodes of Late Paleozoic A-type magmatism in the Qunjisayi area, western Tianshan: petrogenesis and tectonic implications. Journal of Asian Earth Sciences 113, 238–253.
Liang, T., Guo, X., Gao, J., Fan, T., Qin, H., Zhou, R., Hei, H., 2011. Geochemistry and structure characteristic of Carboniferous volcanic rocks in the eastern of Bogeda Mountain. Xinjiang Geology 29, 289–295 (in Chinese with English abstract).
Liu, D.D., Guo, Z.J., Zhang, Z.C., Wu, C.D., 2012. The Late Paleozoic tectonic relationship between the Tian Shan orogenic belt and Junggar basin: constraint from zircon SHRIMP U–Pb dating and geochemistry characteristics of volcanic rocks in Arbasay Formation. Acta Petrologica Sinica 28, 2355–2368 (in Chinese with English abstract).
Liu, H.-Q., Xu, Y.-G., He, B., 2013. Implications from zircon-saturation temperatures and lithological assemblages for Early Permian thermal anomaly in northwest China. Lithos 182–183, 125–133.
Liu, H.-Q., Xu, Y.-G., Tian, W., Zhong, Y.-T., Mundil, R., Li, X.-H., Yang, Y.-H., Luo, Z.-Y., Shang-Guan, S.-M., 2014. Origin of two types of rhyolites in the Tarim Large Igneous Province: consequences of incubation and melting of a mantle plume. Lithos 204, 59–72.
Liu, D.D., Cheng, F., Guo, Z., Jolivet, M., Song, Y., 2015. Lahar facies of the latest Paleozoic Arbasay formation: geomorphological characters and paleoenvironment reconstruction of Northern Tian Shan, NW China. Journal of Asian Earth Sciences 113, 282–292.
Ma, J.C., 1999. Study on the Huangcaopo Group in the eastern Junggar. Journal of Mineralogy and Petrology 19, 52–55 (in Chinese with English abstract).
Ma, R.S., Shu, L.S., Sun, J.Q., 1997. Tectonic Evolution and Metallization in the Eastern Tianshan Belt, China. Geological Publishing House, Beijing, p. 202 (in Chinese with English abstract).
Miller, C.F., McDowell, S.M., Mapes, R.W., 2003. Hot and cold granites? Implications of zircon saturation temperatures and preservation of inheritance. Geology 31, 529–532.
Nesbitt, H.W., Markovics, G., 1997. Weathering of granodioritic crust, long-term storage of elements in weathering profiles, and petrogenesis of siliciclastic sediments. Geochimica et Cosmochimica Acta 61, 1653–1670.
Nesbitt, H.W., Young, G.M., 1982. Early Proterozoic climates and plate motions inferred from major element chemistry of lutites. Nature 299, 715–717.
Obrist-Farner, J., Yang, W., 2015. Nonmarine time-stratigraphy in a rift setting: an example from the Mid-Permian lower Quanzijie low-order cycle, Bogda Mountains, NW China. Journal of Palaeogeography 4, 27–51.
Pearce, J.A., Harris, N.B.W., Tindle, A.G., 1984. Trace element discrimination diagrams for the tectonic interpretation of granitic rocks. Journal of Petrology 25, 956–983.
Peccerillo, A., Barberio, M.R., Yirgu, G., Ayalew, M., Barbieri, D., Wu, T.W., 2003. Relationships between mafic and peralkaline silicic magmatism in continental rift settings: a petrological, geochemical and isotopic study of the Gedemsa Volcano, central Ethiopian rift. Journal of Petrology 44, 2003–2032.
Pin, C., Paquette, J.L., 1997. A mantle-derived bimodal suite in the Hercynian Belt: Nd isotope and trace element evidence for a subduction-related rift origin of the Late Devonian BreÂvenne metavolcanics, Massif Central (France). Contributions to Mineralogy and Petrology 129, 222–238.
Pirajno, F., Mao, J.W., Zhang, Z.C., Zhang, Z.H., Chai, F.M., 2008. The association of mafic–ultramafic intrusions and A-type magmatism in the Tianshan and Altay orogens, NW China: implications for geodynamic evolution and potential for the discovery of new ore deposits. Journal of Asian Earth Sciences 32, 165–183.
Qin, K.Z., Su, B.X., Sakyi, P.A., Tang, D.M., Li, X.H., Sun, H., Xiao, Q.H., Liu, P.P., 2011. SIMS zircon U–Pb geochronology and Sr–Nd isotopes of Ni–Cu-bearing mafic-ultramafic intrusions in eastern Tianshan and Beishan in correlation with flood basalts in Tarim Basin (NW China): constraints on a ca. 280 Ma mantle plume. American Journal of Science 311, 237–260.
Safonova, I., Seltmann, R., Kröener, A., Gladkochub, D., Schulmann, K., Xiao, W., Kim, T., Komiya, T., Sun, M., 2011. A new concept of continental construction in the Central Asian Orogenic Belt (compared to actualistic examples from the Western Pacific). Episodes 34, 186–194.
Safonova, I., Biske, G., Romer, R.L., Seltmann, R., Simonov, V., Maruyama, S., 2016. Middle Paleozoic mafic magmatism and ocean plate stratigraphy of the South Tianshan, Kyrgyzstan. Gondwana Research 30, 236–256.
Sengör, A.M.C., Natal'In, B.A., Burtman, U.S., 1993. Evolution of the Altaid tectonic collage and Palaeozoic crustal growth in Eurasia. Nature 364, 299–307.
Shu, L.S., Zhu, W.B., Wang, B., Faure, M., Charvet, J., Cluzel, D., 2005. The post-collision intracontinental rifting and olistostrome on the southern slope of Bogda Mountains, Xinjiang. Acta Petrologica Sinica 21, 25–36 (in Chinese with English abstract).
Shu, L.S., Wang, B., Zhu, W.B., Guo, Z.J., Charvet, J., Zhang, Y., 2011. Timing of initiation of extension in the Tianshan, based on structural, geochemical and geochronological analyses of bimodal volcanism and olistostrome in the Bogda Shan (NW China). International Journal of Earth Sciences 100, 1647–1663.
Si, G., Su, H., Yang, G., Zhang, C., Yang, G., 2014. Geological significance and geochemical characteristics of the Sikeshu pluton in North Tianshan, Xinjiang. Xinjiang Geology 32, 19–24 (in Chinese with English abstract).
Sparks, R.S.J., Self, S., Walker, G.P.L., 1973. Products of ignimbrite eruptions. Geology 1, 115–118.
Sumner, J.M., Wolff, J., 2003. Petrogenesis of mixed-magma, high-grade, peralkaline ignimbrite 'TL' (Gran Canaria): diverse styles of mingling in a replenished, zoned magma chamber. Journal of Volcanology and Geothermal Research 126, 109–126.

Sun, S.S., McDonough, W.F., 1989. Chemical and isotopic systematics of oceanic basalts: implications for mantle composition and processes. In: Saunders, A.D., Norry, M.J. (Eds.), Magmatism in the Ocean Basins. Geological Society Special Publications, pp. 313–345.

Sun, G., Li, J., Gao, L., Yang, T., 2005. Zircon SHRIMP U–Pb age of a dioritic pluton in the Harlik Mountain, Eastern Xinjiang, and its tectonic implication. Geological Review 51, 463–469 (in Chinese with English Abstract).

Tang, G.-J., Wang, Q., Wyman, D.A., Sun, M., Li, Z.-X., Zhao, Z.-H., Sun, W.-D., Jia, X.-H., Jiang, Z.-Q., 2010. Geochronology and geochemistry of Late Paleozoic magmatic rocks in the Lamasu-Dabata area, northwestern Tianshan (west China): evidence for a tectonic transition form arc to post-collisional setting. Lithos 119, 393–411.

Tang, G.-J., Wang, Q., Wyman, D.A., Li, Z.-X., Zhao, Z.-H., Yang, Y.-H., 2012. Late Carboniferous high εNd(t)-εHf(t) granitoids, enclaves and dikes in western Junggar, NW China: ridge-subduction-related magmatism and crustal growth. Lithos 140–141, 86–102.

Tang, G.-J., Chung, S.-L., Wang, Q., Wyman, D.A., Dan, W., Chen, H.-Y., Zhao, Z.-H., 2014. Petrogenesis of a Late Carboniferous mafic dike-granitoid association in the western Tianshan: response to the geodynamics of oceanic subduction. Lithos 202–203, 85–89.

Thy, P., Beard, J.S., Lofgred, G., 1990. Experimental constraints on the origin of Icelandic rhyolites. Journal of Geology 98, 417–421.

Tong, Y., Wang, T., Hong, D., Han, B., Zhang, J., Shi, X., Wang, C., 2010. Spatial and temporal distribution of the Carboniferous–Permian granitoids in northern Xinjiang and its adjacent areas, and its tectonic significance. Acta Petrologica et Mineralogica 29, 619–641 (in Chinese with English Abstract).

Troll, V.R., Schmincke, H.-U., 2002. Magma mingling and crustal recycling recorded in ternary feldspar from compositionally zoned peralkaline ignimbrite 'A', Gran Canaria, Canary Islands. Journal of Petrology 43, 243–270.

Walker, G.P.L., 1983. Ignimbrite types and ignimbrite problems. Journal of Volcanology and Geothermal Research 17, 65–88.

Wan, M.-L., Zhou, W.-M., Yang, W., Wang, J., 2016. Charred wood of *Prototaxoxylon* from the Wuchiapingian Wutonggou Formation (Permian) of Dalongkou, northern Bogda Mountains, northwestern China. Palaeoworld 25, 21–31.

Wang, B.Y., Jiang, C.Y., Li, Y.J., Wu, H.E., Xia, Z.D., Lu, R.H., 2009. Geochemistry and tectonic implications of Karamaili ophiolite in east Junggar of Xinjiang. Journal of Mineralogy and Petrology 9, 74–82 (in Chinese with English abstract).

Wang, B., Shu, L., Faure, M., Jahn, B.-m., Cluzel, D., Charvet, J., Chung, S.L., Meffre, S., 2011. Paleozoic tectonics of the southern Chinese Tianshan: insights from structural, chronological and geochemical studies of the Heiyingshan ophiolitic mélange (NW China). Tectonophysics 497, 85–104.

Wang, F., Liao, Q., Fan, G., Cheng, W., Tian, J., Chen, S., Wu, W., Hu, C., 2015. Geological implications of unconformity between Upper and Middle Devonian, and 346.8 Ma post-collision volcanic rocks in Karamaili, Xinjiang. Earth Science-Journal of China University of Geosciences 39, 1243–1257 (in Chinese with English abstract).

Wartes, M.A., Carroll, A.R., Greene, T.J., 2002. Permian sedimentary record of the Turpan–Hami basin and adjacent regions, northwest China: constraints on postamalgamation tectonic evolution. Geological Society of America Bulletin 114, 131–152.

Watson, E.B., Harrison, T.M., 1983. Zircon saturation revisited: temperature and composition effects in a variety of crustal magma types. Earth and Planetary Science Letters 64, 295–304.

Whalen, J.B., Currie, K.L., Chappell, B.W., 1987. A-type granites: geochemical characteristics, discrimination and petrogenesis. Contributions to Mineralogy and Petrology 95, 407–419.

Wilhem, C., Windley, B.F., Stampfli, G.M., 2012. The Altaids of Central Aisa: a tectonic and evolutionary innovative review. Earth-Science Reviews 113, 303–341.

Windley, B.F., Alexeiev, D., Xiao, W., Kröner, A., Badarch, G., 2007. Tectonic models for accretion of the Central Orogenic Belt. Journal of the Geological Society, London 164, 31–47.

Xia, L.-Q., Xia, Z.-C., Xu, X.-Y., Li, X.-M., Ma, Z.-P., 2008. Relative contributions of crust and mantle to the generation of the Tianshan Carboniferous rift-related basic lavas, northwestern China. Journal of Asian Earth Sciences 31, 357–378.

Xia, L.-Q., Xu, X.-Y., Li, X.-M., Ma, Z.-P., Xia, Z.-C., 2012. Reassessment of petrogenesis of Carboniferous–Early Permian rift-related volcanic rocks in the Chinese Tianshan and its neighboring areas. Geoscience Frontiers 3, 445–471.

Xiao, W.-J., Zhang, L.-C., Qin, K.-Z., Sun, S., Li, J.-L., 2004. Paleozoic accretionary and collisional tectonics of the Eastern Tianshan (China): implications for the continental growth of Central Asia. American Journal of Science 304, 370–395.

Xiao, W., Han, C., Yuan, C., Sun, M., Lin, S., Chen, H., Li, Z., Li, J., Sun, S., 2008. Middle Cambrian to Permian subduction-related accretionary orogenesis of Northern Xinjiang, NW China: implications for the tectonic evolution of Central Asia. Journal of Asian Earth Sciences 32, 102–117.

Xiao, W., Windley, B.F., Allen, M.B., Han, C., 2013. Paleozoic multiple accretionary and collisional tectonics of the Chinese Tianshan orogenic collage. Gondwana Research 23, 1316–1341.

Xie, W., Xu, Y.-G., Luo, Z.-Y., Chen, Y.-B., Hong, L.-B., Ma, L., Ma, Q., 2016a. Petrogenesis and geochemistry of the Late Carboniferous rear-arc (or back-arc) pillow basaltic lava in the Bogda Mountains, Chinese North Tianshan. Lithos 244, 30–42.

Xie, W., Xu, Y.-G., Chen, Y.-B., Luo, Z.-Y., Hong, L.-B., Ma, L., Liu, H.-Q., 2016b. High-alumina basalts from Bogda Mountains suggest an arc setting for Chinese Northern Tianshan during the Late Carboniferous. Lithos 256–257, 165–181.

Xu, X., Li, X., Ma, Z., Xia, L., Xia, Z., Pen, G., 2006a. LA-ICPMS zircon U–Pb dating of gabbro from the Bayingou ophiolite in the northern Tianshan Mountains. Acta Geologica Sinica 80, 1168–1176 (in Chinese with English abstract).

Xu, X., Xia, L., Ma, Z., Wang, Y., Xia, Z., Li, X., Wang, L., 2006b. SHRIMP zircon U–Pb geochronology of the plagiogranites from Bayingou ophiolite in North Tianshan Mountains and the petrogenesis of the ophiolite. Acta Petrologica Sinica 22, 83–94 (in Chinese with English abstract).

Xu, Q.-Q., Ji, J.-Q., Zhao, L., Gong, J.-F., Zhou, J., He, G.-Q., Zhong, D.-L., Wang, J.D., Griffiths, L., 2013. Tectonic evolution and continental crust growth of Northern Xinjiang in northwestern China: remnant ocean model. Earth-Science Reviews 126, 178–205.

Xu, Y.-G., Wei, X., Luo, Z.-Y., Liu, H.-Q., Cao, J., 2014. The Early Permian Tarim Large Igneous Province: main characteristics and a plume incubation model. Lithos 204, 20–35.

Yang, S.F., Li, Z.L., Chen, H.L., Santosh, M., Dong, C.W., Yu, X., 2007. Permian bimodal dyke of Tarim Basin, NW China: geochemical characteristics and tectonic implications. Gondwana Research 12, 113–120.

Yang, G., Li, Y., Safonova, I., Yi, S., Tong, L., Seltmann, R., 2014. Early Carboniferous volcanic rocks of West Junggar in the western Central Asian Orogenic Belt: implications for a supra-subduction system. International Geology Review 56, 823–844.

Yang, G., Xiao, L., Wang, G., Gao, R., He, X., Zhang, L., Zhou, P., 2015. Geochronological, geochemical and petrogenesis of Bieluagaxi granodioritic pluton in Western Junggar. Earth Science-Journal of China University of Geosciences 40, 810–823 (in Chinese with English abstract).

Yuan, C., Sun, M., Wilde, S., Xiao, W.J., Xu, Y.G., Long, X.P., Zhao, G.C., 2010. Postcollisional plutons in the Balikun area, East Chinese Tianshan: evolving magmatism in response to extension and slab break-off. Lithos 119, 269–288.

Zhang, C.-L., Zou, H.-B., 2013. Permian A-type granites in Tarim and western part of Central Asian Orogenic Belt (CAOB): genetically related to a common Permian mantle plume? Lithos 172–173, 47–60.

Zhang, C.L., Li, X.H., Li, Z.X., Ye, H.M., Li, C.N., 2008. A Permian layered intrusive complex in the western Tarim Block, northwestern China: product of a Ca. 275 Ma mantle plume? The Journal of Geology 116, 269–287.

Zhang, D., Zhang, Z., Santosh, M., Cheng, Z., Huang, H., Kang, J., 2013. Perovskite and baddeleyite from kimberlitic intrusions in the Tarim large igneous province signal the onset of an end-Carboniferous mantle plume. Earth and Planetary Science Letters 361, 238–248.

Zhang, W., Chen, H., Han, J., Zhao, L., Huang, J., Yang, J., Yan, X., 2015. Geochronology and geochemistry of igneous rocks in the Bailingshan area: implications for the tectonic setting of Late Paleozoic magmatism and iron skarn mineralization in the eastern Tianshan, NW China. Gondwana Research. http://dx.doi.org/10.1016/j.gr.2015.10.011.

Zhang, Y., Yuan, C., Long, X., Sun, M., Huang, Z., Du, L., Wang, X., 2016. Carboniferous bimodal volcanic rocks in the eastern Tianshan, NW Chian: evidence for arc rifting. Gondwana Research. http://dx.doi.org/10.1016/j.gr.2016.02.004.

Zhao, T., Xu, S., Zhu, Z., Liu, X., Chen, C., 2014. Geological and geochemical features of Carboniferous volcanic rocks in Bogda–Harlik Mountains, Xinjiang and their tectonic significance. Geological Review 60, 115–124 (in Chinese with English abstract).

Zhong, Y.-T., Xu, Y.-G., 2009. Characteristics of plume-related A-type granites: an example from the Emeishan Large Igneous Province. Journal of Jilin University (Earth Science Edition) 39, 828–838 (in Chinese with English abstract).

Zhou, M.F., Zhao, J.H., Jiang, C.Y., Gao, J.F., Wang, W., Yang, S.H., 2009. OIB-like, heterogeneous mantle sources of Permian basaltic magmatism in the western Tarim Basin, NW China: implications for a possible Permian large igneous province. Lithos 113, 583–594.

Zhu, Y., Guo, X., Song, B., Zhang, L., Gu, L., 2009. Petrology, Sr–Nd–Hf isotopic geochemistry and zircon chronology of the Late Palaeozoic volcanic rocks in the southwestern Tianshan Mountains, Xinjiang, NW China. Journal of the Geological Society, London 166, 1085–1099.

Zindler, A., Hart, S., 1986. Chemial geodynamics. Annual Review of Earth and Planetary Sciences 14, 493–571.